

Hydromorphological response of heavily modified rivers to flood releases from reservoirs: A case study of the Spöl River, Switzerland

Saman Hashemi  | Jonathan Carrivick  | Megan Klaar

School of Geography and Water@leeds,
University of Leeds, Leeds, UK

Correspondence

Saman Hashemi, School of Geography,
University of Leeds, Woodhouse Lane, Leeds,
LS2 9JT, UK.
Email: saman.hashemi02@gmail.com

Funding information

European Union's Horizon 2020 Research and
Innovation Programme under the Marie
Skłodowska-Curie grant Agreement (MSCA),
Grant/Award Number: 765553

Abstract

Releasing experimental floods as part of environmental flow programs aims to restore river beds by moving and restoring sediments to improve hydromorphological conditions of the river. However, it remains a challenge to understand how flood release characteristics affect channel morphology, sediment transport, and hydrodynamics. In this study, field surveys and a 2D hydro-morphodynamic and sediment transport numerical model were used to determine how differences in flood magnitude and falling limb alter hydrogeomorphic conditions within a 4 km reach of the lower Spöl River. The model was constrained by drone flight-derived high-resolution digital elevation models and two field-measured flood releases. The highest flood magnitude of 40 m³/s resulted in 2,700 m³ of total sediment transport, 2,000 m³ of net total volumetric change and 16 900 m² more wetted area after the flood. The same flood, simulated with an increase in falling limb slope, resulted in a decrease in the duration of full sediment mobility and a corresponding reduction of 8% in net total volumetric change and 5.3% in the total wetted area. Contrastingly, the lowest flood magnitude of 25 m³/s produced 130% lower total sediment transport, 105% lower net total volumetric changes and 10% less wetted area after the flood. Overall, we show that hydro-morphodynamic modelling of river erosion and deposition combined with spatially rich topographic datasets are extremely useful in forming designed environmental flood scenarios to optimise sediment transport and thus hydrogeomorphic changes to set environmental flows. We contend that scenario modelling is necessary to help water managers optimise the amount of water allocated to environmental flows and to simultaneously restore and maintain riverine dynamics in heavily modified rivers.

KEYWORDS

channel morphology, Delft3D, environmental flow, experimental flood, hydraulic conditions, sediment transport

1 | INTRODUCTION

Approximately 50% of large rivers globally have been moderately or heavily modified due to flow alteration by dams and over-allocation of water for ever-increasing human demands (Grill et al., 2015; Lehner et al., 2011). These modifications can lead to adverse ecological

changes and degradation (Nilsson et al., 2005; Stewardson et al., 2017) due to severe hydromorphological alteration, including disrupting sediment transport dynamics and shifts in the magnitude, timing and frequency of critical components of the flow regime (Poff et al., 1997).

One of the most promising approaches to support ecological integrity in heavily modified rivers is the concept of “designer flows”

This is an open access article under the terms of the [Creative Commons Attribution-NonCommercial-NoDerivs](https://creativecommons.org/licenses/by-nc-nd/4.0/) License, which permits use and distribution in any medium, provided the original work is properly cited, the use is non-commercial and no modifications or adaptations are made.

© 2023 The Authors. *Earth Surface Processes and Landforms* published by John Wiley & Sons Ltd.

(sensu Acreman et al., 2014) which aims to define and quantify the key components of the flow hydrograph which can be replicated as flow releases from upstream impoundments to create an environmental flow (hereafter called e-flow) regime. Designed flow releases seek to trigger important functional processes (Chen & Olden, 2017), which may otherwise be missing in modified rivers, as mimicking the full natural flow regime is not an appropriate management goal at these sites (Poff, 2018).

Floods are one of the key components of natural river systems heavily controlled by dam operation and diminished by water withdrawals that causes detrimental impacts on the ecological processes downstream of dams (Gregory et al., 2018). Flood events can induce considerable sediment transport (Wohl et al., 2015) and geomorphological changes (Death et al., 2015), which in turn influence hydrodynamics (Guan et al., 2015) and flow complexity patterns (Cao & Carling, 2002; Keylock et al., 2012; Rueda, 2015). In the river environment, hydrodynamic conditions (particularly during flood) are one of the most important features of instream habitat (Dunbar et al., 2012). Complex flow patterns play a significant role in species habitat preferences (Crowder & Diplas, 2006; Kozarek et al., 2010) and are often characterised by a multitude of metrics. These metrics include vorticity (Crowder & Diplas, 2002; Lacey et al., 2012; Wilkes et al., 2013), turbulent kinetic energy (TKE) (Lacey et al., 2012; Li et al., 2019; Li et al., 2020; Silva et al., 2020), Froude number (Boavida et al., 2011; Schlunegger & Garefalakis, 2018) and shear stress (Engelund & Fredsøe, 1976; Meyer-Peter & Müller, 1948; Parker, 1990; Prancevic & Lamb, 2015; Shields, 1936; Wilcock & Crowe, 2003). Thus, floods play a crucial role in improving hydraulic conditions in terms of geomorphological complexity (Bestgen et al., 2020; Gostner, 2012; Yarnell et al., 2015) and river ecological health (Bunn & Arthington, 2002; Richter, 2010; Robinson et al., 2018) by influencing hydromorphological conditions. There is, therefore, a clear need to maintain and, where necessary, to improve the hydromorphological and ecological conditions of river systems.

Designed experimental floods (also named controlled, artificial, and managed floods; Gillespie et al., 2015) have increasingly been used throughout the world to enhance river ecosystem integrity in heavily modified rivers. Releases of experimental floods as part of environmental flow (e-flow) programs have been conducted in a number of river systems around the world, including the United States (Cross et al., 2011; Patten et al., 2001; Schmidt et al., 2001; Shafroth et al., 2010), Switzerland (Mürle et al., 2003; Robinson, 2012; Robinson et al., 2018), France (Loire, Piégay, et al., 2019), Spain (Magdaleno, 2017), New Zealand (Lessard et al., 2013) and Australia (Coleman & Williams, 2017). These releases predominantly aimed to improve the geomorphological and ecological conditions of the rivers by promoting sediment transport within the river (Scheurer & Molinari, 2003). In the long-term, those improvements can sustain the ecological integrity of regulated rivers (Robinson et al., 2018).

Despite the importance of flood events to river health, examining their hydromorphological impacts has been largely ignored in e-flow studies (Gregory et al., 2018; Rose et al., 2020; Wohl et al., 2015). Moreover, it remains a challenge to understand how flood characteristics (e.g. magnitude, duration and falling limb) affect channel morphology, sediment transport and hydrodynamics (Kaur et al., 2019; Konrad et al., 2011; Phillips et al., 2018). Only a few studies have investigated the effect of flood characteristics on sediment transport (Batalla &

Vericat, 2009; Eaton & Lapointe, 2001; Mao, 2012; Phillips et al., 2018). Given recent stresses on water resources in many parts of the world, it is difficult for water managers to deal with the complexity of allocating water resources to various downstream demands (Cosgrove & Loucks, 2015). It is therefore vitally important to quantify the effect of key elements of a flood hydrograph in terms of magnitude and rate of change and (re)design them to improve hydromorphological conditions while minimising the amount of water released.

This study applies a 2D hydro-morphodynamic model to experimental flood releases to qualify the spatiotemporal effect of flood characteristics (peak magnitude and falling limb rate) on hydromorphological processes and resulting complexity within a heavily modified Alpine waterbody (the Spöl River, Switzerland). Various hydraulic and morphologic parameters were extracted to investigate the possible differences that changing the input hydrograph would make on river flow pattern and morphology. We performed a comparative analysis of six different flood scenarios to clarify and improve experimental flow releases within the e-flow program to maximise hydromorphological conditions and water release. The objectives of this study are as follows: (i) to quantify spatiotemporal variation of hydromorphological changes that occurred within and after flood events, (ii) to assess how flow magnitude and rate of change of the falling limb of the experimental flood hydrograph affect sediment transport dynamics and flow structure, with a focus on hydromorphological processes and (iii) to determine which aspects of the experimental flood releases are most important in driving increased sediment transport and resultant bed morphology changes (erosion and deposition of sediment).

2 | STUDY SITE

This study exploits a wealth of pre- and postexperimental flood data available at the Lower Spöl River, downstream of the Ova Spin reservoir. The Spöl River is an alpine river located in Switzerland in the protected area of Swiss National Park (Figure 1). The source of the Spöl River is in the Forcola di Livigno at 2315 m above sea level in Italy. The river consists of two sections of the regulated river,

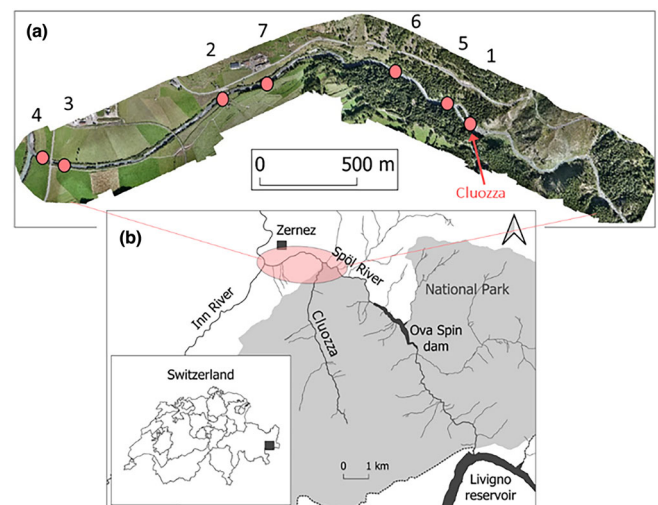


FIGURE 1 (a) Drone-based image of the study reach and sampling points where hydromorphological data was collected (flow direction from right to left) and (b) map of the lower Spöl River. [Color figure can be viewed at [wileyonlinelibrary.com](https://onlinelibrary.wiley.com/terms-and-conditions)]

dominated by the Livigno and Ova Spin reservoirs which operate as storage systems for hydropower production, and only release constant residual flows ($0.9 \text{ m}^3/\text{s}$) below the reservoir except during the experimental floods (Scheurer & Molinari, 2003). The Upper Spöl flows from Livigno reservoir on the border of Italy. The river runs for approximately 5.7 km before entering the Ova Spin reservoir. The Lower Spöl section starts from downstream of the Ova Spin reservoir and merges with the Inn River, which is one of the main tributaries of the Danube River, at the town of Zernez.

This study was conducted on the lower Spöl between Ova Spin reservoir and Inn River confluence (Scheurer & Molinari, 2003). Cluozza is the main tributary of the lower Spöl (Figure 1) and transports significant sediment input to the river (Scheurer & Molinari, 2003). River bed substrate in the lower Spöl is dominated by cobbles and gravels (Kevic et al., 2018). In 1970, flow regulation in the Spöl began and in 2000, a flood program for releasing experimental floods was started by the National Park and the Engadine power company to improve habitat conditions for brown trout (*Salmo trutta*), the only fish inhabiting the river (Ortlepp & Mürle, 2003). Two flood discharges prior to flow regulation occurred in 1979 at $42 \text{ m}^3/\text{s}$ and in 1990 at $33 \text{ m}^3/\text{s}$. Ever since the implementation of the flood program in 2000, experimental floods continue to release one or two times per year in the lower Spöl. The timing and magnitude of the released floods depend on research needs and water availability ranging from 15 to $25 \text{ m}^3/\text{s}$ (1-year return period) to $30\text{--}40 \text{ m}^3/\text{s}$ (10-year return period). The artificial floods are more notable in the lower Spöl for mobilising the river bed of finer sediment (Kevic et al., 2018) which are mainly provided by the Cluozza tributary. The duration of floods is usually between 6 and 8 hours with a peak duration of 2–3 hours. These flood releases do not act as sediment flushing flows as they are released from the top of the dam, therefore contribute very little sediment to the system and predominantly only mobilise sediment that is already in the river. More details about the hydromorphological conditions of the river before the dam was built are in Uehlinger et al. (2003) and Robinson et al. (2018). The experimental floods analysed in this research were two artificial flood releases on 4 September 2018 with a magnitude of $25 \text{ m}^3/\text{s}$ and 8 hours' duration and on 24 June 2019 with magnitude $40 \text{ m}^3/\text{s}$ and 11 hr duration, downstream of Ova Spin reservoir into the lower Spöl.

3 | MATERIALS AND METHODS

The main tool available for modelling hydromorphological processes within rivers is numerical modelling. Current understanding of hydromorphological processes of flood events is largely based on the application of these models (Guan et al., 2014; Li et al., 2014; Li & Duffy, 2011; Simpson & Castelltort, 2006; Tavelli et al., 2020; Wong et al., 2015; Xia et al., 2010). Over the past two decades, the use of numerical modelling to connect ecology to hydromorphological processes has increased (Escobar-Arias & Pasternack, 2010; Gaeuman, 2014; Lane et al., 2018; Pasternack et al., 2004; Vanzo et al., 2016). However, the application of numerical models for examining hydromorphological impacts of flow regimes and specifically for e-flow is rare but includes Gregory et al. (2018), for example. Moreover, the application of these models to evaluate the effect of hydrograph characteristics of short time-scale and high flow releases (such as

experimental floods) on river hydromorphology has received little attention (Espa et al., 2022). Numerical modelling provides a powerful virtual setup to quantify the impacts of different flow scenarios through simulating flow-sediment interactions. This gives river managers additional flexibility for making decisions about the flow release characteristics, which eventually help them reach environmental objectives, especially in heavily modified rivers where hydromorphological alterations are the primary concern (EU WFD, 2019; Gregory et al., 2018).

3.1 | Hydro-morphodynamic modelling

Delft3D model (version 4.02.03 of the Delft3D modelling package) was selected for this study as it can simulate hydraulic variables and interactions between the flow and sediment transport (Deltares., 2014). Specifically, the physical-based, fully nonlinear, open-source software is an advanced graphically interfaced numerical model that allows simulation of hydro- and morpho-dynamics (Deltares., 2014). The Delft3D-FLOW module (2D) was employed to set up the model and execute the hydro-morphodynamic simulations. Sediment transport and morphological changes were achieved using the Van Rijn (1984) equation for suspended load transport (suspended sediment concentration) and the Meyer-Peter & Müller (1948) equation for bedload transport (Deltares., 2014). Model equations and more details about the Delft3D model are in Lesser et al. (2004) and specifically as applied to morphodynamic modelling of gravel bed rivers in Carrivick (2009); Carrivick et al. (2009, 2010, 2012, 2013); Smith et al. (2014); and Staines & Carrivick (2015). Numerical simulations resulted in the calculation of the hydraulic parameters including depth-averaged velocity, flow depth, Froude number (Fr), bed shear stress (τ) and complexity metrics including vorticity (ω) and TKE for every node of the computational mesh. Vertical river bed changes, that is, morphodynamics (sediment erosion and deposition) were also computed by the model and iteratively updated to feedback affect the hydraulics in the next model time step.

3.1.1 | Field data on hydromorphological parameters

Hydromorphological data including water level, flow velocity and suspended sediment concentration were collected (locations highlighted in Figure 1a; field data are presented in supporting information Data S1 in Figure S1 and Tables S1 and S2) and used for model calibration and modelling flow and sediment transport (Deltares., 2014). Flow velocity was measured using a handheld Decature Surface Velocity Radar (SVR) with $\pm 0.03 \text{ m/s}$ of velocity precision at 0° and $\pm 4^\circ$ of vertical angle precision (Manual, 2019) at nine cross-sectional positions along Wooden Bridge (location 2) during the first flood on 4 September 2018 and seven cross-sectional positions during the 24 June 2019 flood event. SVR estimates are reliant on the selection of a depth-averaged to surface velocity ratio, or velocity coefficient (α). The default α value of 0.85, a widely accepted value employed in many rivers, was selected as the valid confirm value which gives an accurate SVR-based velocity estimate (Welber et al., 2016).

Field sampling to measure suspended sediment concentration for subsequent simulation of suspended sediment transport within the models was conducted by collecting nine water samples (1 L volume of sample bottle) at the Wooden Bridge (location 2) where the flow current was deepest, during the rising and falling limb of the flood hydrograph. The samples were analysed in the laboratory of the University of Trento (Italy) by using settleable solids in Imhoff cones, and results were verified with the calibrated turbidity measures of the laboratory nephelometer. Suspended sediment concentration was used for both upstream and downstream boundary conditions of the model. A Wolman pebble count was conducted in 2018 at three locations (locations 5, 6 and 7, Figure 1a), a minimum of 100 pebbles (from surface river bed) per sample as outlined in Ruiz-Villanueva et al. (2022). Data reported in Ruiz-Villanueva et al. (2022) were received by request and subsequently used to calculate Manning's n roughness, and boundary shear stress thresholds were used as model inputs to analyse bed movement stages. D50 and D90 bed surface grain sizes were used as the sediment input in the model. Two water level data loggers (In-Situ Rugged Troll 100 with $\pm 0.05\%$ precision) were installed at the Wooden Bridge (location 2) and the Road Bridge (location 3). Water level data were logged in 15-minute time intervals before, during and after the flood and were used as the model boundary conditions.

Three cross-sections were employed to illustrate the detail of hydro-morphodynamic simulation from the most upstream to most downstream cross-sections. The most upstream cross-section (location 1, Figure 1) was located after the Cluozza tributary, the mid-stream cross-section (location 7) was located before the Wooden Bridge and the most downstream cross-section (location 4) was located before the confluence of the Spöl River with the River Inn near the model boundary. These cross-sections were used to show the downstream variation of hydraulic variables.

3.1.2 | Topographic data

A drone flight was conducted before and after the 4 September 2018 flood event (Figure 1a) to provide high-resolution (< 0.03 m) orthoimages and point cloud data (using ground control points measured with dGPS precision ± 0.05 m) covering a 4 km length and extending, approximately 2.5 km below the Ova Spin reservoir before the main tributary Ova da Cluozza and extending to the confluence with River Inn. Pre- and post-flood topographic data were surveyed on 3 and 11 September 2018, respectively. Since the 2010s, drone flights have been becoming commonplace as a means to collect overlapping optical images from which very high-resolution and high-precision 3D models can be made of complex surfaces (Carrivick et al., 2016; James et al., 2019; Woodget et al., 2017). The drone images consisted of a digital camera mounted onto a WingtraOne drone. Sensor specifications are a Sony Rx1r2 camera (normal model) with sensor dimensions of 35.000 (mm) \times 23.345 (mm), camera image size 7952 \times 5304 (RGB), effective focal length of 7470.428 (pixel) 32.880 (mm), prime lens type and global sensor shutter type. The drone was positioned at 240 m above ground level, and images were collected with a high level of overlap ($> 75\%$). A total of 24 GCPs (ground control points) were randomly distributed across the site, and their positions were recorded using dGPS technique. Field condition was blue sky and slightly windy, and ground sampling distance was 0.024 m. Number of

images that have been used for the reconstruction of the model was 735 and all images enabled. The raw images were processed with Structure-from-Motion technique (Westoby et al., 2012) using Pix4D (version 4.2.17) to create point cloud and orthoimages. The precision of the orthoimages is ± 0.1 m, and point cloud spacing is typically < 0.1 m. The camera model parameters were optimised within bundle block adjustment (Carrivick et al., 2016). The principal points (CO_x and CO_y) were approximately half the resolution of the camera, and the radial distortion values (R1, R2 and R3) were smaller than 1. The uncertainties on the focal length and the principal points were negligible (only a few pixels). The uncertainties on the distortion parameters (R1, R2 and R3) were close to zero. Tangential distortion parameters (T1 and T2) of the lens were zero. Finally, the model performed a high quality calibration as most of the parameters were decorrelated. However, the observed correlation between the radial distortion parameters was expected.

The drone-based point clouds were subsequently used to create digital elevation models (DEMs) as a topographic input for Delft3D model and a DEM of difference (DoD) to calibrate the morphodynamic model. DEMs (XY resolution of 0.5 m for modelling efficiency, retaining Z precision of ± 0.1 m) were generated using an image filtering algorithm approach in ArcGIS software version 10.4.1. Firstly, digital surface models (DSMs) were generated using the point cloud. Filtering of DSMs was carried out using image classification and segmentation to obtain bare-earth data (Pfeifer, 2008; Sammartano & Spanò, 2016). The process required four steps of data preparation, supervised classification analysis (including classifier training), accuracy assessment and DEM generation (DEM generation process explained in more details in the supporting information, Figure S2 and Table S3). A total of 120 field surveyed check points (CPs) were collected along the river thalweg using dGPS and were combined with an image filtering algorithm (Zietara, 2017) to generate accurate DEM in deep, turbid and turbulent water areas (Moretto et al., 2014). For generating DEMs from overlapping images, it is quality and distribution, not quantity of CPs, that is important (Woodget et al., 2017).

3.1.3 | Model setup

The resulting DEM was converted to an XYZ file as topography input for Delft3D, using ArcGIS software version 10.4.1. The Delft3D-RGFGRID module was used to generate a grid with mesh cell size 1*1 m (longitudinal 1 m, and cross-sectional 1 m), and then topography points were mapped into the grid (computational domain and mesh generation is presented in the supporting information Figure S3). Mesh size was selected based on performing mesh independence analysis. The Delft3D-FLOW module was employed to set up the model and execute flow and sediment transport. Ten hours of flow and sediment transport simulation of the base flow (0.9 m³/s) was run to provide an initial condition for the later flood event models. The initial condition allows all cells to be initially considered as wet. Downstream boundaries that define how and where the simulated flow leaves the geometry of the solving field were inserted using field water level measurements. The flow discharge from the Cluozza tributary was also added to the model domain (0.93 m³/s during flood event 2018 and 2.26 m³/s during flood event 2019). We considered sediment in the upstream (u/s) and downstream (d/s) boundary

conditions and inserted sediment flux data at both boundaries into the model. Suspended sediment data were collected on the Wooden Bridge which were used for both u/s and d/s boundary conditions. For bedload, grain size distributions for the surface river bed were collected at three locations, and D50 and D90 were used to represent bed material in the model. The time step for simulating flood scenarios was set as 0.003 min. This was selected based on the Courant number to avoid instabilities and divergence in the simulation (Deltares., 2014).

3.1.4 | Model calibration

Model calibration with field measurements is one of the commonly used approaches to determining model accuracy by adjusting the model inputs to match the model outputs with the measured data. In this study, the hydrodynamic model was calibrated by adjusting Manning roughness (n) value and using velocity field measurement data. n values were changed within reasonable ranges (from 0.02 to 0.055), and the simulated velocities were compared with the co-located SVR velocities. The model was calibrated by optimising n values to minimise model error statistics including mean absolute error (MAE) and root mean squared error (RMSE). To assess the accuracy of the model after calibration, model error statistics were used based on the following equations:

$$MAE = \sum_i^n \frac{|x_{mod} - x_{obs}|}{n} \quad (1)$$

$$RMSE = \sqrt{\sum_i^n \frac{(x_{mod} - x_{obs})^2}{n}} \quad (2)$$

where x_{mod} and x_{obs} are simulated and measured variables (e.g. velocity) for i^{th} co-located point at the collected grid cell. The value of the Manning roughness that best replicated the field measurements of flow velocity was then used to simulate different flow scenarios. The morphodynamic model was calibrated based on the construction of DEMs of Differences (DoDs). DoDs were produced by subtracting DEM pairs (Lane et al., 2003) using ArcGIS software version 10.4.1. Similarly, pre-and post-flood topographic data were used to calibrate sediment transport by comparing measured and simulated DoDs, by adjusting Manning's n values to minimise MAE and RMSE. Reasonable Manning's n values for rivers with coarse bed material (gravel, cobble and boulder size) ranging from 0.024 to 0.06 (Arcement & Schneider, 1989). Moreover, a visual comparison was carried out between the spatial distribution of simulated hydraulic parameters and field photos/videos to distinguish between the behaviour of the hydro-morphodynamic simulation and what is observed in nature.

3.2 | Designed flow scenarios

The flood magnitude and falling limb rate of single flood events were examined in order to understand the impact of the real-world flood hydrographs on the Spöl river hydraulics and morphology downstream of the Ova Spin dam. Falling limb rate is most important in fish

stranding risk which is the main danger to fish during the flood process and can increase fish mortality (Espa et al., 2022; Moreira et al., 2019). Scenarios were designed according to operational constraints including available water restrictions and downstream hydraulic conditions. Two groups of scenarios based on two observed flood events were designed and modelled. The first group of scenarios includes Sc1–Sc3. Scenario 1 (Sc1) represents the original flood hydrograph from the observed flood release in 2018 (Table 1 and Figure 2), with a modelled scenario decrease (26%; Sc2) and 100% increase (Sc3) in falling limb rate. The second group includes Sc4–Sc6. Scenario 4 (Sc4, representative of the observed flood event in 2019) was then altered with a decrease (26%, Sc5) and increase (100%, Sc6) in falling limb rate. Sc4 was designed to reflect Sc1 with a constant falling limb rate (2.5 l/s/s), but with an altered peak flow magnitude (37% increase), 100% increase in rising limb rate, and 44% increase in flood duration. Sc5 was designed to reflect Sc2 with a constant falling limb rate (1.85 l/s/s) but with altered flood characteristics similar to the changes made between Sc1 and Sc4. Sc6 reflects Sc3 with a 100% increase in rising limb rate and 61% increase in flood duration. A 60-min step in the rising limb of the Sc4 and Sc6 hydrograph was designed to model the real-world operational constraints (e.g. maximum allowable water volume to be released and downstream safety) faced during large flood events. This time step is the time needed for receiving confirmation of the safety of the downstream Wooden Bridge before further increasing the discharge. The rising limb of the Sc5 does not contain the 60-min step due to the combination of creating a gentle falling limb and available water volume to be released.

Kruskal–Wallis tests and post hoc Wilcoxon Signed Rank tests were used to identify the significant differences between spatial-temporal data (erosion and sedimentation) under different scenarios, using R software (version 3.6.3).

3.3 | Equations for the fluvial physical process

To better understand the changes in the flow pattern and sediment transport, we used the concept of Fr number and bed shear stress, respectively. Although both variables were simulated by the numerical model at each node in the computational mesh, the Fr thresholds (formula 3) were determined based on the concept of subcritical, supercritical and critical flow conditions, and bed shear stress thresholds were calculated manually in the following to characterize bed mobility stages for a better understanding of the sediment transport behaviour. The bed shear stress thresholds which define bed mobility stages (Escobar-Arias & Pasternack, 2010) were determined based on the concept of the Shields shear stress (using formulas 4 and 5). The critical value of shear stress was extracted from the Shields diagram for each measured grain size fraction including D_5 , D_{16} , D_{50} , D_{90} and D_{95} . Simulated boundary shear stress at each node in the computational mesh was then compared with these thresholds of the bed mobility stages determined using Shields' formula during simulation time steps. To assess the cross-sectional variation of hydraulic and morphologic parameters, three cross-sections (locations 1, 4 and 7, Figure 1a) were employed to illustrate the detail of hydro-morphodynamic simulation from most upstream to most downstream reach. The effective wetted area (WA) of computational cells under a given discharge was also

TABLE 1 Hydrograph characteristics of the released (Sc1 and Sc4) and designed flow scenarios (Sc2, Sc3, Sc5 and Sc6) at the Lower Spöl River, downstream of the Ova Spin reservoir.

Flood hydrograph elements	Flood scenarios					
	Sc1	Sc2	Sc3	Sc4	Sc5	Sc6
Base flow (m ³ /s)	0.9	0.9	0.9	0.9	0.9	0.9
Rising limb avg. rate (l/s/s)	2.5	2.5	2.5	5	5	5
Peak flow magnitude (m ³ /s)	25.9	25.9	25.9	40.9	40.9	40.9
Peak duration (minutes)	120	120	120	105	105	105
Falling limb avg. rate (l/s/s)	2.5	1.85	5	2.5	1.85	5
Flood duration (minutes)	480	480	345	690	690	555
Released water vol. (m ³)	457,830	488,682	324,630	1,040,490	992,268	989,550

Note: avg. is average and vol. is volume.

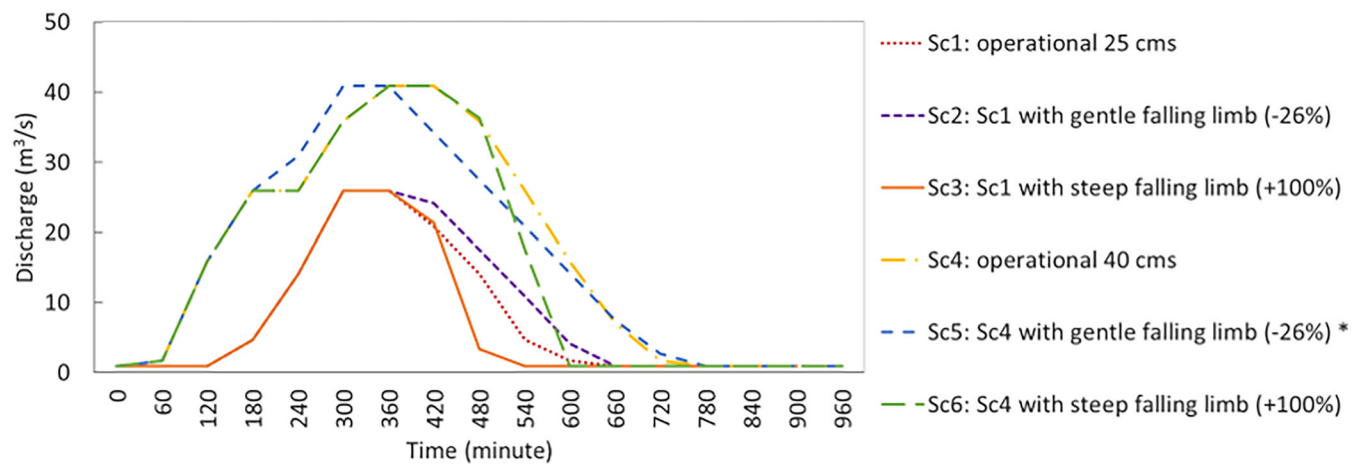


FIGURE 2 Designed flow scenarios for the Spöl River, downstream of the Ova Spin reservoir; cms stands for cubic meters per second; * slope of the rising limb is due to restriction on available water volume to release. [Color figure can be viewed at [wileyonlinelibrary.com](https://onlinelibrary.wiley.com/terms-and-conditions)]

calculated (Antonetti et al., 2023). The Fr, shear stress and WA were calculated according to the following equations (Francalanci et al., 2008; Parasiewicz, 2007):

$$Fr = \frac{V}{(gD)^{0.5}} \quad (3)$$

$$\tau = \frac{\rho V^2}{C_*^2} \quad (4)$$

$$\tau^* = \frac{\tau}{\gamma(G_s - 1)D} \quad (5)$$

$$WA = \sum_{i=1}^n A_i \quad (6)$$

where V = depth averaged velocity (m/s), g = acceleration due to gravity (9.8 m/s²), D = flow depth (m), τ = boundary shear stress which is the variable that best characterizes the strength of the flow around the particle (N/m²), ρ = water density (kg/m³), C_* = dimensionless Chezy coefficient, τ^* = dimensionless critical shear stress, γ = water specific weight (9.807 KN/m³), G_s = sediment specific gravity (assumed to be 2.65), D = sediment grain diameter (mm), WA = wetted area (m²) and A_i = area of i^{th} computational cell.

To compare bed elevation changes between different flood scenarios induced by flood geomorphic processes, 'net deposition', 'net erosion' and 'net change' were determined for each scenario. The net deposition was computed as the sum of positive cells computed from the first and last DEM. The net erosion was calculated as the sum of negative cells computed from the first and last DEM. The net change was calculated as the sum of positive and negative cells derived from the first and last DEM.

4 | RESULTS

4.1 | Model calibration

Model calibration using adjusted Manning's n (ranging from 0.02 to 0.055) to minimise MAE and RMSE reveals calculated error statistics for both measured and simulated flow velocity (Figure 3). Manning roughness 0.04 reflected the minimum calculated error statistics. Therefore, this value was selected to have the best model predictive capability. The overall calibration value of 0.04 is comparable with that found in other studies (Carolli et al., 2017; Espa et al., 2015). Comparing modelled DoD generated from Delft3D with measured DoD generated from pre-and post-flood drone-based data, under Sc1, also shows the combination of hydrodynamic modelling and applied

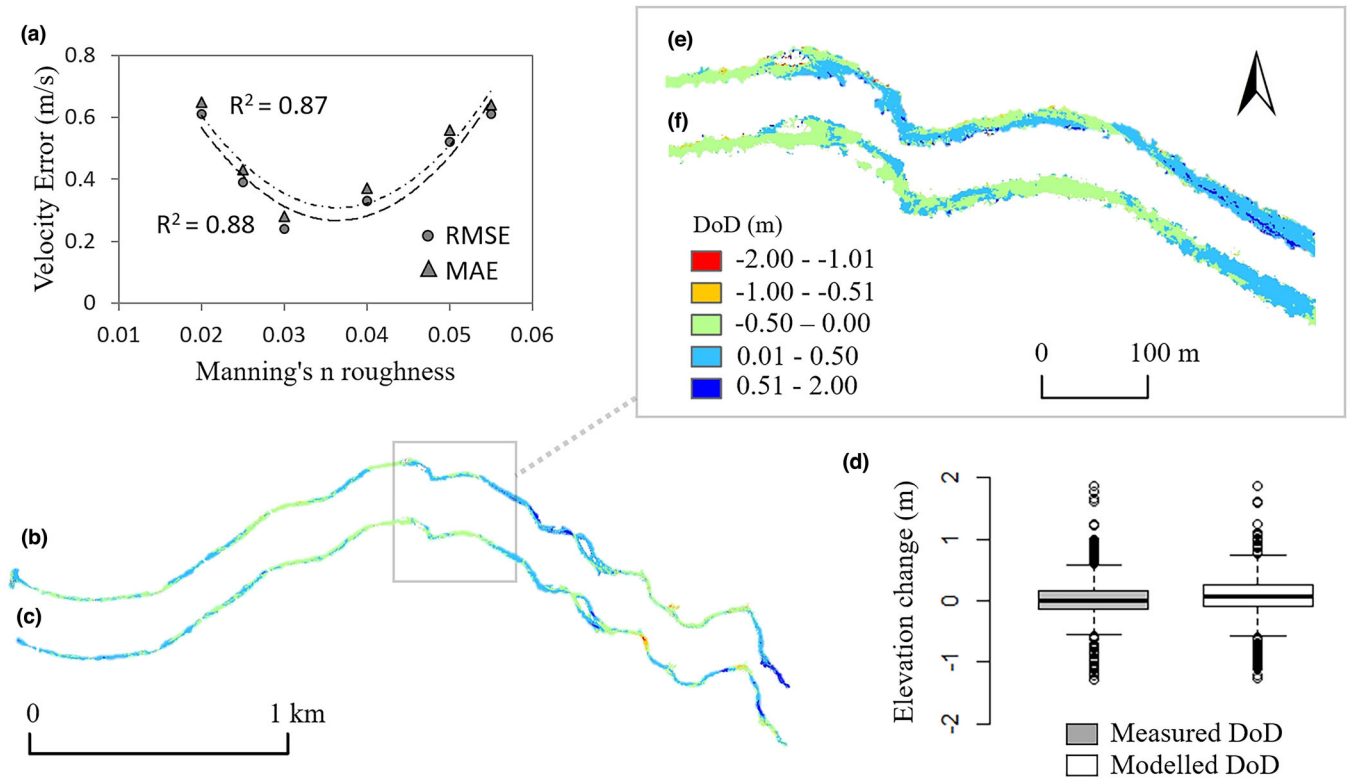


FIGURE 3 (a) Model calibration using velocity errors of measured and modelled flow velocity at the Wooden Bridge, using mean absolute error (MAE) and root mean squared error (RMSE), under Sc1 to calibrate the hydrodynamic model; (b) measured DEM of difference (DoD); (c) modelled DoD under Sc1; (d) difference between measured and modelled DoDs; (e) a close-up of the measured DoD; and (f) a close-up of the modelled DoD. Negative and positive values show erosion and deposition respectively; flow direction from right to left. [Color figure can be viewed at wileyonlinelibrary.com]

bedload transport formula acceptably matched with field measurements (Figure 3). Moreover, a good agreement was found between the behaviour of the hydro-morphodynamic simulation and what is observed in nature (Figure 4).

4.2 | Flood scenario modelling

Hydro-morphodynamic modelling of the six flood scenarios shows a varied response in hydraulic and geomorphological conditions. An increase in flood magnitude from 25 to 40 m³/s (around 60% increase in flood magnitude and 127% increase in total volume of released water from Sc1 to Sc4) resulted in an increase in wetted area by 14% (corresponding to 9,386 m²; details of the total wetted area is presented in the supporting information Table S4). Decreasing the falling limb rate (represented by Sc2 and Sc5), both caused a 1% increase in wetted area compared to Sc1 and Sc4, however, by increasing the falling limb rate from 2.5 to 5 L/s/s in Sc3 and Sc6 respectively, a reduction by 2% and 4% of wetted area occurred. The most profound differences are between Sc1 and Sc4 with two different flood magnitudes and are analysed in Figure 5. According to this figure, the river flow under Sc1 (during the peak flow) reached a velocity of 4.14 m/s, flow depth 2 m, Fr 2.13, bed shear stress 233.8 N/m², vorticity 1.26 1/s and TKE 3.46 m²/s². However, the river flow under Sc4 experienced flow velocity of 5 m/s, flow depth 1.75 m, Fr 2.41, bed shear stress 327.6 N/m², vorticity 2.41 1/s and TKE 5.79 m²/s². The figures for Sc1 also show that the mean hydraulic values changed before and after the floods with velocity from 0.57 m/s (pre-flood condition) to

0.72 m/s (post-flood condition, 900 min after flood initiation), flow depth 0.19 to 0.13 m, Fr 0.44 to 0.59, bed shear stress 10.1 to 13.3 N/m², vorticity 0.48 to 0.7 1/s and TKE 0.009 to 0.006 m²/s². A similar trend has been observed for Sc4.

The overall spatial pattern of hydraulic parameters (Figure 6) shows that the flow pattern is strongly altered after the flood. The floods caused an increase in the flow velocity and total submerged area in the floodplain and change in spatial pattern of bed shear stress and flow complexity metrics.

To illustrate temporal changes in hydraulic conditions between flood scenarios, simulated Fr during floods and the percentages of nodes with various Fr classes were compared in Figure 7. These results show that increasing the rate of the falling limb of the flood hydrographs (Sc3) diminished the variety of flow conditions during the flood, in comparison to Sc1 and Sc2 with the same flow magnitude. Sc3 created 23% (12 999 m²) less wetted area within the range of 0.5 ≤ Fr < 1 (subcritical) in comparison to Sc1 and Sc2. Sc3 also generated 12% (6919 m²) and 17% (9732 m²) fewer mesh nodes within the range of Fr < 0.5 (subcritical) and Fr ≥ 1 (super-critical) in comparison to Sc1 and Sc2. By decreasing the falling limb from Sc1 to Sc2, 7% (4036 m²) more mesh nodes with Fr > 0.5 are created.

The same case applied to Sc6 (with Q_{peak} = 40 m³/s) when comparing this scenario with Sc4 and Sc5 with the same peak flow magnitude. This scenario generated 13% (7,496 m²), 25% (13,771 m²) and 8% (4,613 m²) fewer mesh nodes with range Fr < 0.5, 0.5 ≤ Fr < 1 and Fr ≥ 1 in comparison to Sc4 and Sc5. By increasing in the peak flow magnitude, Sc4 (with Q_{peak} = 40 m³/s) in comparison to the Sc1 (with Q_{peak} = 25 m³/s) has 12% (7,137 m²), 47% (26,974 m²) and

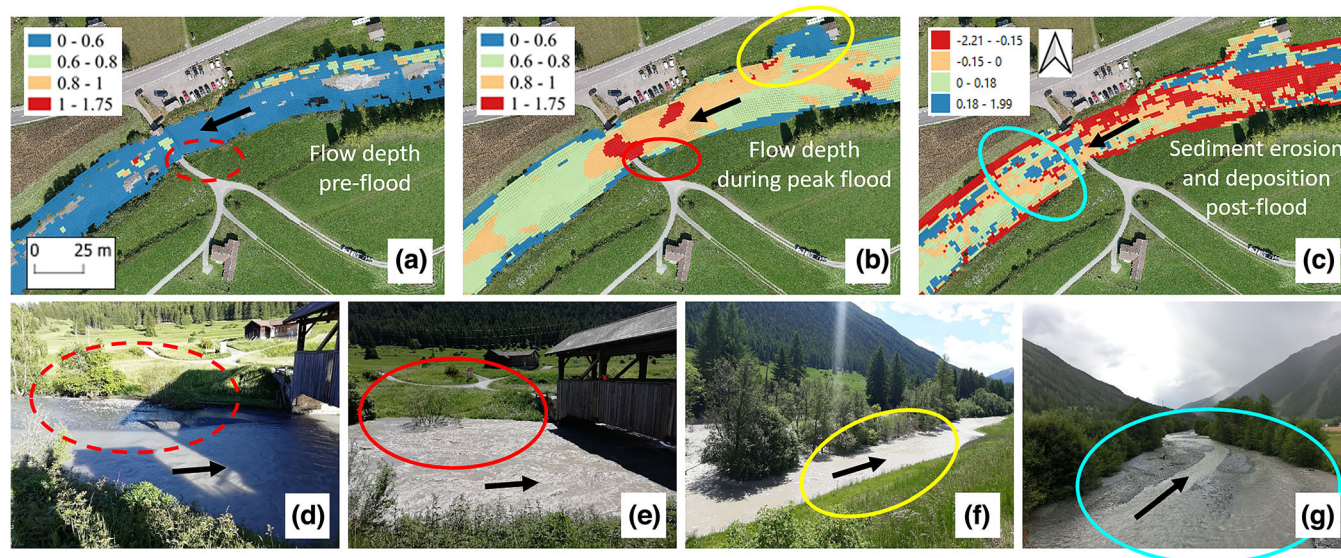


FIGURE 4 Visual comparison between the spatial distribution of simulated hydraulic parameters (a, b, c) and field photos (d, e, f, g); (a) simulated water depth before the flood; (b) simulated water depth during flood Sc4; (c) simulated sediment erosion and deposition after flood Sc4; (d) before flood Sc4; (e and f) during flood Sc4; and (g) after flood Sc4. Arrows show the flow direction. Circles with similar colours show corresponding locations in the model and nature. Comparing figures a and b with d and e (water level changes at the left river bank before Wooden Bridge) represents a good agreement between the hydro-morphodynamic simulation and what is observed in nature; this agreement can also be observable by looking at yellow circles which shows the same location of an inundated area in model and nature. The light blue circle in figure c presents sediment erosion and deposition patterns in much the same pattern as is in figure g. [Color figure can be viewed at wileyonlinelibrary.com]

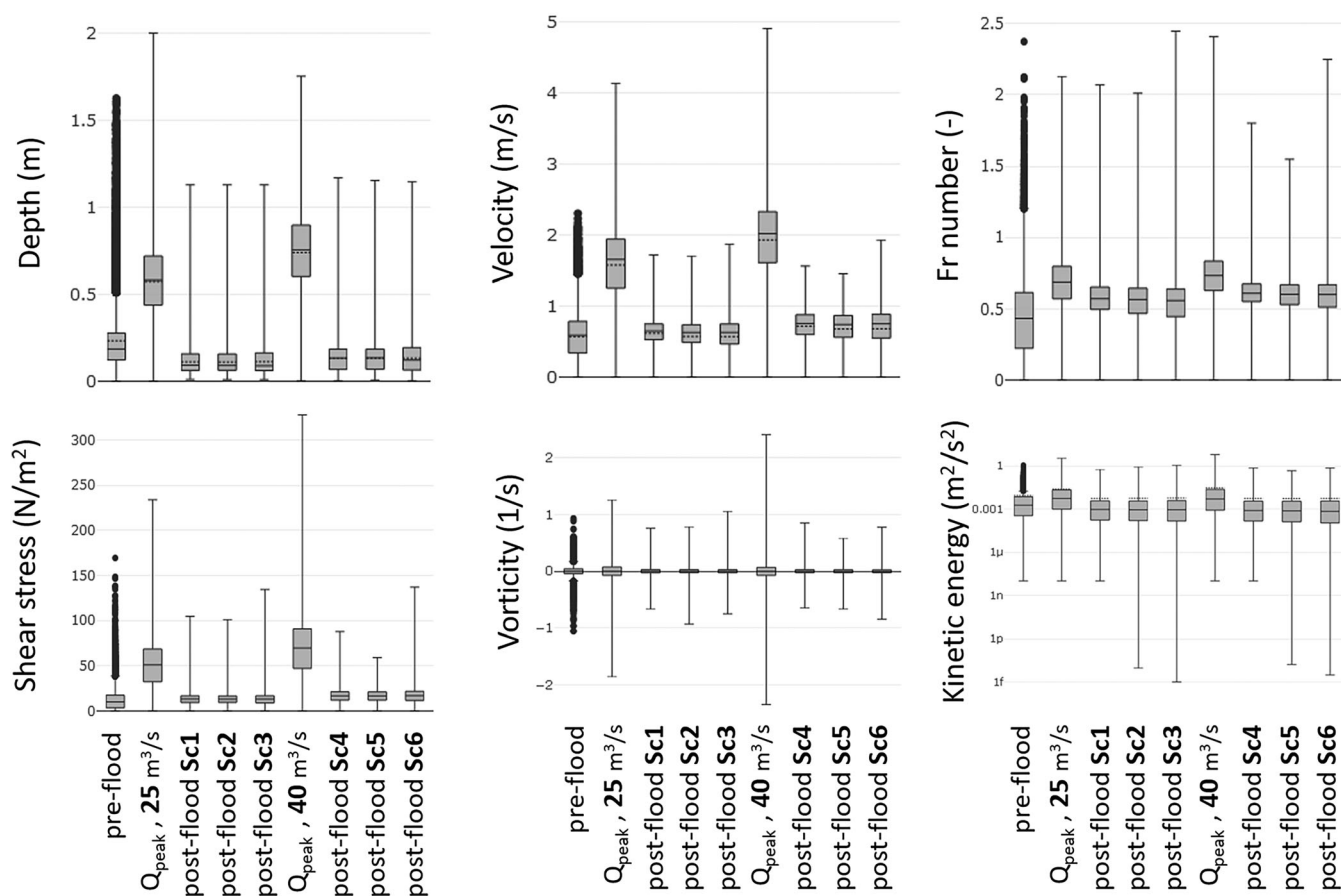


FIGURE 5 Descriptive summaries of multiple hydraulic variables for pre-flood, peak flood (360 min after flood initiation) and post-flood (900 min after flood initiation) conditions for the entire river reach under all flood scenarios.

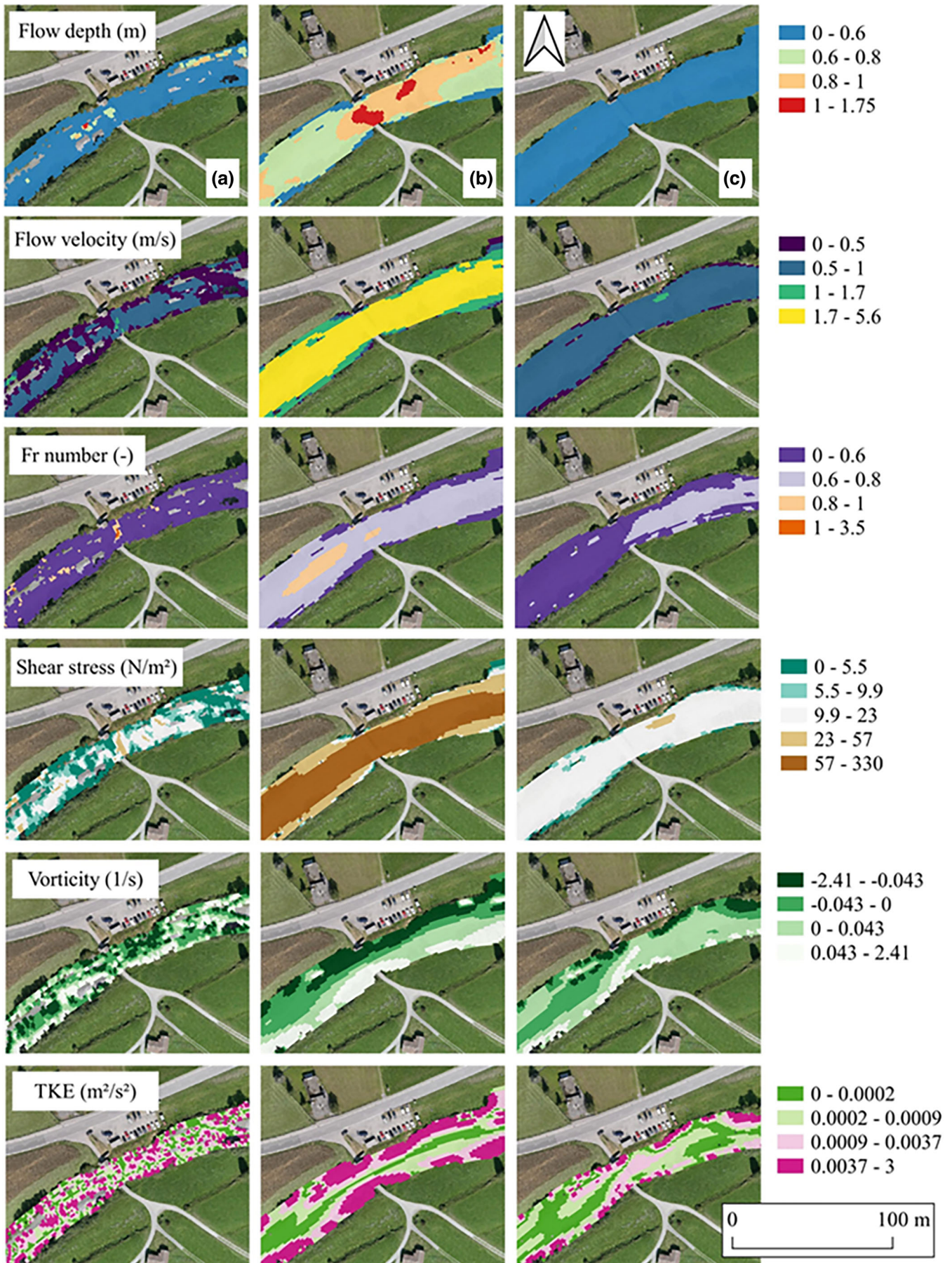


FIGURE 6 Detailed example view of simulated hydraulic parameters under Sc_4 ($Q_{\text{peak}} = 40 \text{ m}^3/\text{s}$) near the Wooden Bridge; (a) pre-flood, (b) during peak flood and (c) post-flood conditions; flow direction from right to left. [Color figure can be viewed at [wileyonlinelibrary.com](https://onlinelibrary.wiley.com)]

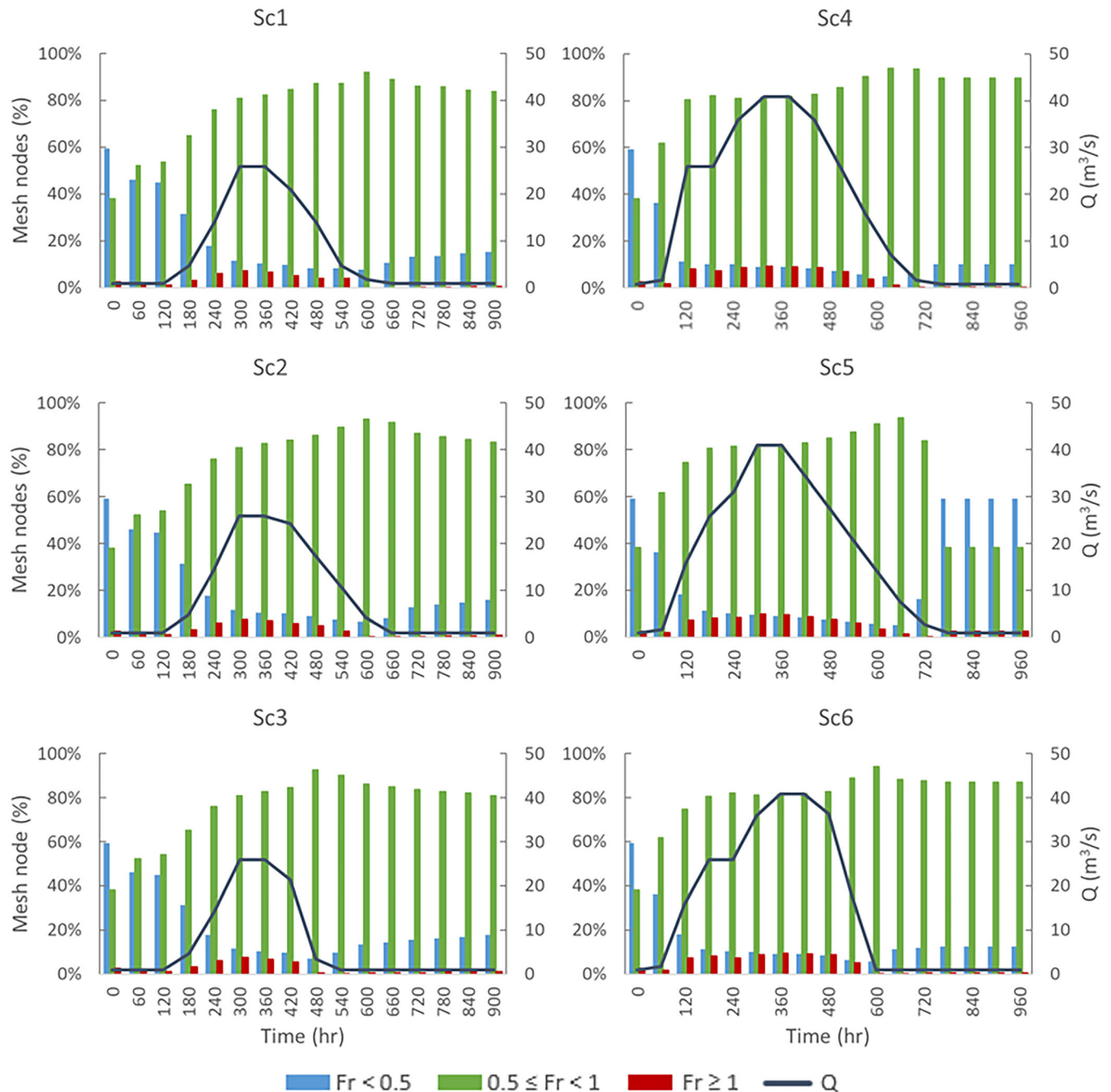


FIGURE 7 Percentages of the number of cells within Fr number classes per the total count of wet nodes under Sc1, Sc2 and Sc3 with $Q = 25 \text{ m}^3/\text{s}$ and Sc4, Sc5 and Sc6 with $Q = 40 \text{ m}^3/\text{s}$. [Color figure can be viewed at [wileyonlinelibrary.com](https://onlinelibrary.wiley.com)]

91% ($52,545 \text{ m}^2$) more areas with $Fr < 0.5$, $0.5 \leq Fr < 1$ and $Fr \geq 1$ thresholds, respectively.

4.3 | Morphodynamic variation

Calculation of the critical shear stress (See supporting information Table S5) shows the entrainment thresholds required to move different grain size fractions and various phases of sediment transport including fine, medium, coarse and very coarse gravel mobility stages. Simulated boundary shear stress at each node in the computational mesh compared with the thresholds of the bed mobility stages during different time steps (Figure 8) resulted in boundary bed shear stress

thresholds of $5.5 \leq \tau < 9.9$ for washing fine gravel stage, $9.9 \leq \tau < 23$ for medium gravel movement stage and $23 \leq \tau < 57$ and $\tau \geq 57$ for the full mobility stage.

Increasing the rate of the falling limb (Sc3) resulted in a reduction in the percentage of mesh nodes within a specific shear stress threshold for the entire simulation area. Sc3 involved the river bed 37% less in the full mobility ($23 \leq \tau < 57$ and $\tau \geq 57$), 43% less in the medium gravel movement ($9.9 \leq \tau < 23$) and 46% less in the fine gravel mobility ($5.5 \leq \tau < 9.9$) in comparison to Sc1. Similarly, Sc6 involved the river bed in 18% less in the full mobility stage, 35% less in the medium gravel movement stage and 22% less in the washing fine gravel stage, in comparison to Sc4. By increasing the magnitude of the flood in Sc4, the number of mesh nodes with full mobility increased by 42%

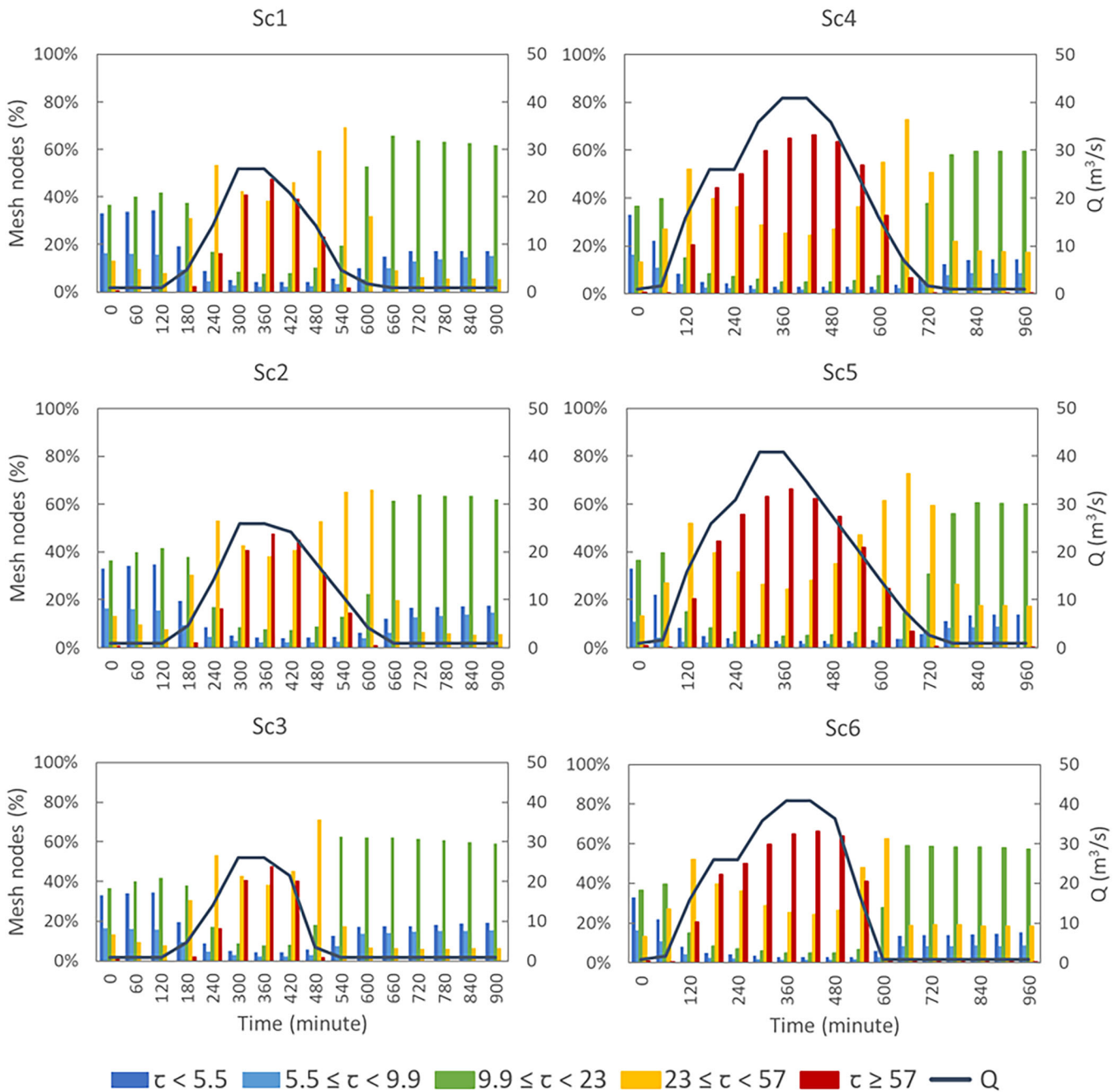


FIGURE 8 Percentages of cells within entrainment thresholds per the total count of wet nodes under Sc1, Sc2 and Sc3 with $Q = 25 \text{ m}^3/\text{s}$ and Sc4, Sc5 and Sc6 with $Q = 40 \text{ m}^3/\text{s}$. [Color figure can be viewed at wileyonlinelibrary.com]

(24,382 m^2 wetted area), and fine gravel mobility increased by 4% (2,450 m^2), but the number of mesh nodes of medium gravel mobility decreased for 7% (4,263 m^2) in comparison to Sc1.

The transport of sediment particles during simulated flood events was divided into suspended load and bedload. Table 2 presents a cross-sectional variation of total load, suspended load and bedload transport volume (m^3) for two upstream (U/S) and downstream (D/S) cross-sections (Cross-sections 1 and 4 are shown in Figure 1; more information on bed elevations at the cross-sections is provided in the supporting information Figure S4) under all flood scenarios. Cumulative sediment transport shows that in all cases the suspended load accounts for 76% to 87% of total sediment. By increasing flow magnitude (comparison of Sc1 and Sc4), the total volume of transported

sediment increased from 1,172 to 2,695 m^3 (an increase of 130%) in the upstream cross-section. Increasing the flow magnitude did not equally contribute to increasing suspended and bedload transport.

It resulted in a 170% increase in the transported bedload volume and a 120% increase in the transported suspended load volume. By decreasing the rate of the falling limb in Sc2 (compared to Sc1), there was an increase in the rate of the total sediment, suspended load, and bedload transport by 12.3%, 13.2% and 8.5%, respectively. However, increasing the rate of the falling limb in the Sc3 caused a decrease in the rate of the total sediment, suspended load and bedload transport by 13.2%, 14.2% and 12.8%, respectively. All flood scenarios represented an average decrease in the total transported sediment volume by 47% towards the end of the reach.

TABLE 2 Cumulative sediment transport (m^3) for both upstream (U/S) and downstream (D/S) cross-sections in post-flood condition (900 min after flood initiation); local peak Q includes Cluozza discharge.

Flood scenario	Location	Flow discharge characteristics		Cumulative volume (m^3)		
		Local peak Q (m^3/s)	Falling limb rate (L/s/s)	Total transport	Bedload	Suspended load
Sc1	U/S	26.83	2.5	1172.3	232.9	939.3
	D/S	26.83	2.5	615.6	77.7	537.9
Sc2	U/S	26.83	1.85	1316.4	252.8	1063.6
	D/S	26.83	1.8	707.6	93.3	614.3
Sc3	U/S	26.83	5	1018.0	199.8	819.0
	D/S	26.83	5	526.4	68.6	457.8
Sc4	U/S	43.16	2.5	2694.9	628.4	2066.4
	D/S	43.16	2.5	1447.8	267.7	1180.0
Sc5	U/S	43.16	1.85	2605.9	592.5	2013.3
	D/S	43.16	1.85	1371.3	239.0	1132.3
Sc6	U/S	43.16	5	2422.6	581.8	1840.7
	D/S	43.16	5	1281.8	243.7	1038.0

Interplay effects between the flow and bed morphology are observable in sedimentation and net elevation change. The median net elevation change and net total volumetric change are shown in Figure 9 and Table 3 under all flood scenarios. There was a difference between Sc1 (953 m^3) and Sc2 ($1,048 \text{ m}^3$) of 10% in volumetric changes. The difference between Sc1 (953 m^3) and Sc3 (885 m^3) was a 7% change. The difference between Sc4 ($1,956 \text{ m}^3$) and Sc5 ($1,984 \text{ m}^3$) was just 2%, and between Sc4 and Sc6 ($1,795 \text{ m}^3$) was 8%. Comparing net total volumetric changes between Sc4 and Sc1 resulted in just over a doubling (105%). Median net elevation change between scenarios with the same peak flood magnitude was not significantly different (0.15 m under Sc1, Sc2 and Sc3, and 0.20 m under Sc4, Sc5 and Sc6). Contrastingly, there was a 33% change between Sc1 (0.15 m) and Sc4 (0.20 m).

Moreover, the results of the Kruskal–Wallis test ($p < 0.001$) on spatial and temporal variation of erosion and deposition indicated significant differences between scenarios, with a post hoc pairwise Wilcoxon test ($p < 0.001$ for all the tests) indicating that all scenarios are significantly different from one another. Therefore, changing down-ramping rates resulted in changes in the spatial–temporal variation of sediment erosion and deposition which are significantly different under different scenarios.

5 | DISCUSSION

Using the detailed streambed topography and experimental flood release conditions found at the Spöl River, it was possible to use two experimental flood releases to calibrate and validate a 2D hydro-morphodynamic model. The model was subsequently used to estimate how alterations to the flood magnitude and falling limb (using modelled scenarios) altered hydraulic and geomorphological conditions within the study reach. In general, the modelled flood scenarios were found to be highly informative.

5.1 | Effect of the flood magnitude on hydro-morphodynamic conditions

The difference between the measured DoD and the simulated DoD showed the patterns of field and modelled DoDs were identical. Comparison of the hydro-morphodynamic model results with the field observations shows that sediment transport and the resultant morphological change affected the wetted area extent and the flow pattern within the Spöl River. More interestingly, the flood enhanced spatial heterogeneity of flow complexity metrics (e.g. vorticity and TKE). With a 60% increase in flood magnitude from Sc1 to Sc4 (from 25 to 40 m^3/s with a similar falling limb rate), the wetted areas (Table S4) corresponding to available velocity, Fr and bed shear stress ranges increased by 9,160 m^2 , wetted area corresponds to vorticity and TKE values raised by 9,386 m^2 and net total volumetric change raised by 1,002 m^3 (Table 3). These findings are similar to those found by Schlosser (1995) who reported that extreme high discharges increased the length of the stream edge and perimeter of the lateral flow areas. Wright and Kaplinski (2011) and Rueda (2015) stated that the flood hydrograph characteristics (such as peak discharge and falling limb) could strongly influence the flow complexity metrics, affecting channel morphology by altering bed shear stress and sediment transport. This increase in wetted area is important in creating spatial heterogeneity in flow pattern and hydraulic conditions as determined by hydromorphological diversity. This result is also consistent with Van Appledorn et al. (2019), who documented the effect of floods on wetted areas caused by morphologic changes.

The modelling has also shown that the floods increased net total volumetric changes and led to hydromorphological modifications. Results from simulating two different flood magnitudes showed that increasing the flood magnitude increased the net total volumetric change by more than double (Table 3). This suggests that the 40 m^3/s floods have more sediment transport capacity than the smaller 25 m^3/s floods and moved larger sediment particles as bedload. The

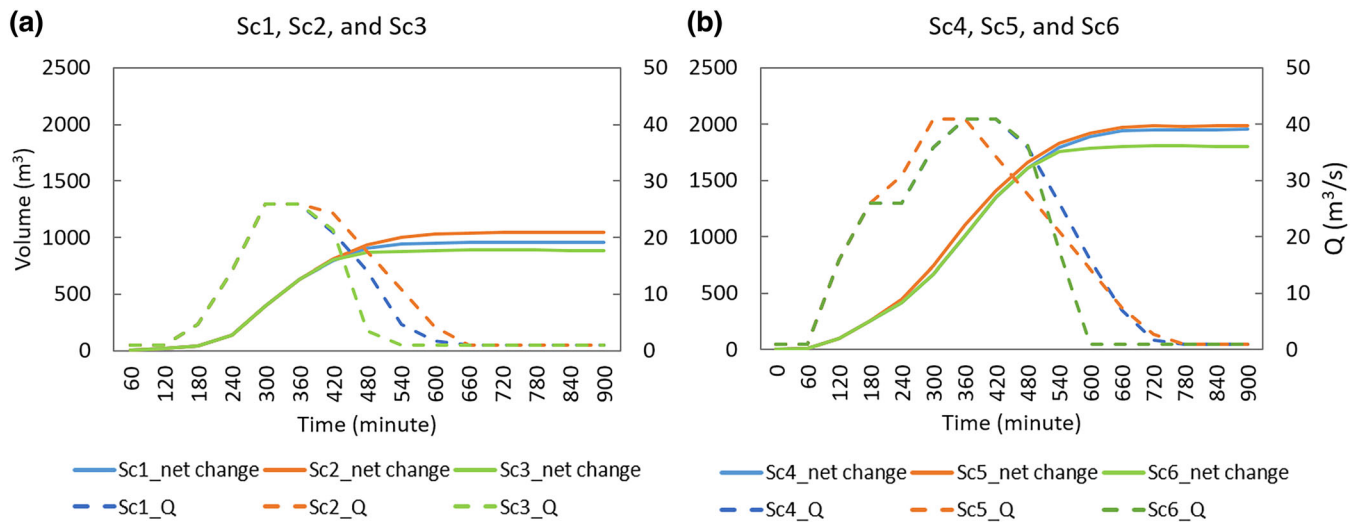


FIGURE 9 Net total volumetric change for the entire study reach at different time steps under (a) 25 m³/s and (b) 40 m³/s flood scenarios. [Color figure can be viewed at wileyonlinelibrary.com]

TABLE 3 Net sediment deposition, erosion, and change under Sc1–Sc6 for the entire study reach.

Topographic change	ΔZ_{\sim} (m)	ΣVol (m ³)	ΔZ_{\sim} (m)	ΣVol (m ³)	ΔZ_{\sim} (m)	ΣVol (m ³)
	Sc1		Sc2		Sc3	
Net deposition	0.154	8008	0.158	8215	0.150	7813
Net erosion	−0.142	−7054	−0.144	−7167	−0.137	−6928
Net change	0.15	953	0.15	1048	0.14	885
	Sc4		Sc5		Sc6	
Net deposition	0.206	11,532	0.206	11,433	0.199	11,261
Net erosion	−0.188	−9576	−0.186	−9450	−0.188	−9466
Net change	0.20	1956	0.20	1984	0.19	1795

Note: ΔZ_{\sim} is the median net elevation change and ΣVol is the net total volumetric change of all numerical cells in the computational domain. Deposition and erosion refer to aggradation and degradation, respectively.

increase in sediment mobility observed in the both magnitude flood events is likely to have enhanced geomorphological complexity by transporting sediment and driving sediment erosion and deposition to create a new flow and hydraulic conditions (Lane et al., 2020; Wyrick et al., 2014). In addition, Gostner (2012) found that hydromorphological changes had a significant impact on the ecological function of the river ecosystem. Future work should assess the effect of such morphological changes on enhancing aquatic habitat ecological conditions. Median net elevation change under different peak flood magnitudes was not significantly different (Table 3). Pfeiffer et al. (2019) observed that the relationship between peak flood magnitude and the bed elevation change is not linear, and bed elevation might show little or even zero response to the highest peak discharge. In other words, they noted that there is a lack of a relationship between flood magnitude and changing bed elevation. This highlights the need for carefully designed experimental flood releases (Lane et al., 2020; Loire, Grosprêtre, et al., 2019). In this context, an essential benefit of morphodynamic modelling is that it quantifies erosion and deposition during a flood and for different flow scenarios that would otherwise be unobtainable.

The complexity of the flow pattern is strongly altered after the floods due to sediment transport, erosion, deposition and changes in bed morphology (as shown in Figure 6). Before the floods, low flows created many patches. In contrast, the floods readjusted the river bed morphology and reworked the river bed, leaving a more uniform gravel extent. For instance, the spatial pattern of TKE showed significant improvement in post-flood conditions compared to pre-flood conditions. This is because of the effect of flood on the river bed morphology (Tamminga et al., 2015). The interaction between sediment erosion and deposition (induced by changes in shear stress) and altered flow complexity metrics (i.e. vorticity and turbulent flows) changed spatial extent of gravels. Future work should investigate the effect of complexity flow metrics on enhancing river habitat heterogeneity after releasing experimental floods. Studies show that too much erosion can lead to scouring and washing organisms out (Downes & Street, 2005), while deposition of large quantities of sediment can lead to burial (Conroy et al., 2018; Wood, 2005). The ability to design and model appropriate flood hydrographs helps improve the amount and distribution of geomorphological structures without too much scouring or sediment deposition and also reducing the pressure on

the reservoir water volume (Lenzi & Marchi, 2000; Rainato et al., 2018).

Based on the results, increasing the flow magnitude during the rising limb of the hydrograph (Table 2) had a more effect on bedload transport than suspended load (nearly more than 20%), even though suspended load counts for 76% to 87% of the total sediment transport in all flood scenarios. This aligns with Hsu et al. (2011) and Rueda (2015) reported suspended and bedload transport that differs on the rising and falling limbs. This could be because the smaller flood magnitudes already transported suspended sediment as the flow is above the threshold of fine particle transport. In contrast, larger floods were associated with a longer flow duration above the threshold of coarse sediment motion which transports bedload.

5.2 | Effect of the falling limb

The rate of falling limbs of flood releases greatly influenced sediment transport and morphological changes in the downstream river. In gravel bed rivers, the falling limb rate organises the spatial distribution of substrate, and this organisation can have a significant impact on bed morphology and resulting hydraulic conditions (Newson & Newson, 2000). The decline in the sediment deposition and available wetted areas due to the increasing falling limb rate may reflect the fact that it affects river bed morphology and bed development processes (Hayes et al., 2019; Mao, 2012; Pitt & Kendy, 2017; Staines & Carrivick, 2015; Welcomme & Halls, 2004). Therefore, to create a dynamic hydraulic condition and minimise the risk of fish stranding, it would be more ecologically suitable to design the falling limb of a flood to be gradual enough to permit the complete reworking of bed morphology (Hayes et al., 2019). Additional effort should be conducted in future research to model fish drift and stranding within the Spöl, including validation with observed fish data.

Similarly, a reduction in the falling limb slope (increasing duration of falling limb represented by Sc2 and Sc5; Figure 9 and Table 3) led to increased net total volumetric change and extended post-flood wetted areas. Comparing the temporal pattern of bed shear stress revealed that it remained beyond the mobility threshold even during the hydrograph's falling limb, which means the falling limb still influences sediment transport, although the flow discharge is declining. The results show that a more gradual falling limb keeps high shear stress (more than the mobility threshold) for a more extended period, which causes the river bed to experience sediment entrainment mobility much longer (Figure 8). Therefore, the falling limb's slope and duration play an essential role in the sediment transport volume and bed morphology after the peak flood (Hassan et al., 2006; Stähly et al., 2020).

Comparing results between downstream and upstream cross-sections (Table 2) revealed that all flood scenarios caused more suspended and bedload transport in upstream cross-sections than in the downstream sections. Additionally, it is evident from the results that a lower falling limb slope eventually increased the total transported sediment through the whole system. This longitudinal pattern indicates that some mobilised sediment was subsequently stored within the study reach, rather than being fully evacuated, which could mean that the falling limb's duration affects both sediment transport

and bed morphology. Spatial and temporal variation in sediment transport within two cross-sections in a river reach has been reported in other studies (Liedermann et al., 2018; Wohl & Cenderelli, 2000).

5.3 | Designing experimental floods

In this study, real-world constraints were part of the design choice, including the maximum authorised water volume and peak flow to release to avoid the river experiencing a floodplain inundation downstream of the River where there are agricultural farms and also endangered the Wooden Bridge's safety. The magnitude of this flood scale (i.e. bank-full 1.6–2 year return period) was a small flood compared to what a natural river may experience. It is critical to the habitat if it never receives a floodplain flood and only in small bank-full floods. However, it seems that there is a threshold of flood magnitude that enables sediment transport and prolongs this (shallower recession limb) and therefore allows more bed change. These design criteria and thresholds could be taken into account by reservoir managers.

6 | CONCLUSION

Using 2D numerical modelling to simulate flood scenarios, this study found releasing higher flood peak magnitude caused more net total bed volumetric change. However, releasing a lower flood peak (25 m³/s rather than 40 m³/s) magnitude may be sufficient to flush sediment and improve hydromorphological conditions and the complexity of flow patterns in the Spöl River. We also found that the falling limb is an important feature of the flood regime in changing spatial patterns of bed morphology to create a dynamic flow pattern. Distribution of TKE along the river showed significant improvements of flow complexity pattern in post-flood conditions compared to pre-flood condition. Preferring any released flood over another one depends lastly on the objectives and operational goals of the release. Alternative objectives may include higher sediment transport regime or reworking existing river bed morphology to maximize flow heterogeneity as observed in this study.

The results presented in this paper illustrate the importance of using high-resolution geomorphologic datasets coupled with hydro-morphodynamic models. This allows the design of experimental floods simply not only by considering the available flow (Whipple & Viers, 2019) but also by considering other key ecological metrics such as sediment transport, river bed morphology (Ashworth & Ferguson, 1986) and flow complexity metrics. Modelling sediment transport and changes in river bed morphology is imperative because the interaction of the two sets of processes determines hydraulics and flow complexity metrics. Therefore, taking these interactions into account when designing high flow releases from reservoirs is critical, particularly in heavily modified rivers, which are substantially changed in hydromorphological character (Acreman et al., 2014). The work presented here provides information and tools for river managers to optimise flood release programs that improve hydromorphological conditions considering water resource availability and operational constraints in the River Spöl.

AUTHOR CONTRIBUTIONS

SH: conceptualization, resources, methodology, data curation, formal analysis, visualization, field investigations and provision of data, software, writing the original draft & editing the manuscript. JC and MK: conceptualization, resources, methodology, software, reviewing & editing the manuscript and supervision.

ACKNOWLEDGEMENTS

This research is part of the Euro-FLOW project (EUROpean training and research network for environmental FLOW management in river basins) funded by the European Union's Horizon 2020 Research and Innovation Programme under the Marie Skłodowska-Curie grant Agreement (MSCA) no. 765553. This study was made possible with the help of the Swiss National Park. We greatly appreciate Michael Doering (ZHAW and eQcharta GmbH) and Dr. Virginia Ruiz-Villanueva (University of Lausanne) for data support, Tulio Soto (University of Trento) for field and data support, and Johannes Ortlepp (Hydra GmbH) for the planning of the floods, hydrological data and his thoughtful comments. All authors declare that they have no conflicts of interest.

DATA AVAILABILITY STATEMENT

The data that support the findings of this study are available from the corresponding author upon reasonable request.

ORCID

Saman Hashemi  <https://orcid.org/0000-0001-7095-6735>

Jonathan Carrivick  <https://orcid.org/0000-0002-9286-5348>

REFERENCES

- Acreman, M., Arthington, A.H., Colloff, M.J., Couch, C., Crossman, N.D., Dyer, F., et al. (2014) Environmental flows for natural, hybrid, and novel riverine ecosystems in a changing world. *Frontiers in Ecology and the Environment*, 12(8), 466–473. Available from: <https://doi.org/10.1890/130134>
- Antonetti, M., Hoppler, L., Tonolla, D., Vanzo, D., Schmid, M. & Doering, M. (2023) Integrating two-dimensional water temperature simulations into a fish habitat model to improve hydro-and thermopeaking impact assessment. *River Research and Applications*, 39(3), 501–521. Available from: <https://doi.org/10.1002/rra.4043>
- Arcement, G.J. & Schneider, V.R. (1989) Guide for selecting Manning's roughness coefficients for natural channels and flood plains. Water Supply Paper 2339. Washington, DC: US government printing office. Available from: <https://doi.org/10.3133/wsp2339>.
- Ashworth, P.J. & Ferguson, R.I. (1986) Interrelationships of channel processes, changes and sediments in a proglacial braided river. *Geografiska Annaler. Series A, Physical Geography*, 68(4), 361–371. Available from: <https://doi.org/10.1080/04353676.1986.11880186>
- Batalla, R.J. & Vericat, D. (2009) Hydrological and sediment transport dynamics of flushing flows: implications for management in large Mediterranean rivers. *River Research and Applications*, 25(3), 297–314. Available from: <https://doi.org/10.1002/rra.1160>
- Bestgen, K.R., Poff, N.L., Baker, D.W., Bledsoe, B.P., Merritt, D.M., Lorie, M., et al. (2020) Designing flows to enhance ecosystem functioning in heavily altered rivers. *Ecological Applications*, 30(1), e02005. Available from: <https://doi.org/10.1002/eap.2005>
- Boavida, I., Santos, J.M., Pinheiro, A.N. & Ferreira, M.T. (2011) Fish habitat availability simulations using different morphological variables. *Limnetica*, 30(2), 0393–0404. Available from: <https://doi.org/10.23818/limn.30.28>
- Bunn, S.E. & Arthington, A.H. (2002) Basic principles and ecological consequences of altered flow regimes for aquatic biodiversity. *Environmental Management*, 30(4), 492–507. Available from: <https://doi.org/10.1007/s00267-002-2737-0>
- Cao, Z. & Carling, P.A. (2002) A critical reflection of computational fluid dynamics applications to fluvial sedimentary systems. In: Dyer, F.J., Thoms, M.C. & Olley, J.M. (Eds.) *In the structure, function and management implications of fluvial sedimentary systems (Proceedings and Reports)*. IAHS Press, pp. 463–470.
- Carrolli, M., Zolezzi, G., Geneletti, D., Siviglia, A., Carrolli, F. & Cainelli, O. (2017) Modelling white-water rafting suitability in a hydropower regulated Alpine River. *Science of the Total Environment*, 579, 1035–1049. Available from: <https://doi.org/10.1016/j.scitotenv.2016.11.049>
- Carrivick, J. (2009) In: Burr, D.M., Carling, P.A. & Baker, V.R. (Eds.) *Jökulhlaups from Kverkfjöll volcano, Iceland: modelling transient hydraulic phenomena. Megaflooding on Earth and Mars*. Cambridge: Cambridge University Press, pp. 273–289 <https://doi.org/10.1017/CBO9780511635632.015>
- Carrivick, J.L., Brown, L.E., Hannah, D.M. & Turner, A.G.D. (2012) Numerical modelling of spatio-temporal thermal heterogeneity in a complex river system. *Journal of Hydrology*, 414, 491–502. Available from: <https://doi.org/10.1016/j.jhydrol.2011.11.026>
- Carrivick, J.L., Manville, V. & Cronin, S.J. (2009) A fluid dynamics approach to modelling the 18th March 2007 lahar at Mt. Ruapehu, New Zealand. *Bulletin of Volcanology*, 71(2), 153–169. Available from: <https://doi.org/10.1007/s00445-008-0213-2>
- Carrivick, J.L., Manville, V., Graettinger, A. & Cronin, S.J. (2010) Coupled fluid dynamics-sediment transport modelling of a Crater Lake break-out lahar: Mt. Ruapehu, New Zealand. *Journal of Hydrology*, 388(3–4), 399–413. Available from: <https://doi.org/10.1016/j.jhydrol.2010.05.023>
- Carrivick, J.L., Smith, M.W. & Quincey, D.J. (2016) *Structure from motion in the geosciences*. Chichester, UK: Wiley-Blackwell. ISBN: 9781118895818.
- Carrivick, J.L., Turner, A.G.D., Russell, A.J., Ingeman-Nielsen, T. & Yde, J.C. (2013) Outburst flood evolution at Russell Glacier, western Greenland: effects of a bedrock channel cascade with intermediary lakes. *Quaternary Science Reviews*, 67, 39–58. Available from: <https://doi.org/10.1016/j.quascirev.2013.01.023>
- Chen, W. & Olden, J.D. (2017) Designing flows to resolve human and environmental water needs in a dam-regulated river. *Nature Communications*, 8(1), 2158. Available from: <https://doi.org/10.1038/s41467-017-02226-4>
- Coleman, D. & Williams, S. (2017) Mobilising fine sediment in a highly regulated upland snowmelt river using hydrological scaled experimental floods. *Marine and Freshwater Research*, 68(1), 146–158. Available from: <https://doi.org/10.1071/MF15231>
- Conroy, E., Turner, J.N., Rymaszewicz, A., Bruen, M., O'Sullivan, J.J., Lawler, D.M., et al. (2018) Further insights into the responses of macroinvertebrate species to burial by sediment. *Hydrobiologia*, 805(1), 399–411. Available from: <https://doi.org/10.1007/s10750-017-3328-7>
- Cosgrove, W.J. & Loucks, D.P. (2015) Water management: current and future challenges and research directions. *Water Resources Research*, 51(6), 4823–4839. Available from: <https://doi.org/10.1002/2014WR016869>
- Cross, W.F., Baxter, C.V., Donner, K.C., Rosi-Marshall, E.J., Kennedy, T.A., Hall, R.O., Jr., et al. (2011) Ecosystem ecology meets adaptive management: food web response to a controlled flood on the Colorado River, Glen canyon. *Ecological Applications*, 21(6), 2016–2033. Available from: <https://doi.org/10.1890/10-1719.1>
- Crowder, D.W. & Diplas, P. (2002) Vorticity and circulation: spatial metrics for evaluating flow complexity in stream habitats. *Canadian Journal of Fisheries and Aquatic Sciences*, 59(4), 633–645. Available from: <https://doi.org/10.1139/f02-037>
- Crowder, D.W. & Diplas, P. (2006) Applying spatial hydraulic principles to quantify stream habitat. *River Research and Applications*, 22(1), 79–89. Available from: <https://doi.org/10.1002/rra.893>
- Death, R.G., Fuller, I.C. & Macklin, M.G. (2015) Resetting the river template: the potential for climate-related extreme floods to transform

- river geomorphology and ecology. *Freshwater Biology*, 60(12), 2477–2496. Available from: <https://doi.org/10.1111/fwb.12639>
- Deltares. (2014) *Delft3D-FLOW user manual: simulation of multidimensional hydrodynamic flows and transport phenomena, including sediments*. Delft, Netherlands: Deltares.
- Downes, B.J. & Street, J.L. (2005) Regrowth or dispersal? Recovery of a freshwater red alga following disturbance at the patch scale. *Austral Ecology*, 30(5), 526–536. Available from: <https://doi.org/10.1111/j.1442-9993.2005.01467.x>
- Dunbar, M.J., Alfredsen, K. & Harby, A. (2012) Hydraulic-habitat modelling for setting environmental river flow needs for salmonids. *Fisheries Management and Ecology*, 19(6), 500–517. Available from: <https://doi.org/10.1111/j.1365-2400.2011.00825.x>
- Eaton, B. & Lapointe, M. (2001) Effects of large floods on sediment transport and reach morphology in the cobble-bed Sainte Marguerite River. *Geomorphology*, 40(3–4), 291–309. Available from: [https://doi.org/10.1016/S0169-555X\(01\)00056-3](https://doi.org/10.1016/S0169-555X(01)00056-3)
- Engelund, F. & Fredsøe, J. (1976) A sediment transport model for straight alluvial channels. *Hydrology Research*, 7(5), 293–306. Available from: <https://doi.org/10.2166/nh.1976.0019>
- Escobar-Arias, M. & Pasternack, G.B. (2010) A hydrogeomorphic dynamics approach to assess in-stream ecological functionality using the functional flows model, part 1—model characteristics. *River Research and Applications*, 26(9), 1103–1128. Available from: <https://doi.org/10.1002/rra.1316>
- Espa, P., Crosa, G., Gentili, G., Quadroni, S. & Petts, G. (2015) Downstream ecological impacts of controlled sediment flushing in an Alpine valley river: a case study. *River Research and Applications*, 31(8), 931–942. Available from: <https://doi.org/10.1002/rra.2788>
- Espa, P., Petaccia, G., Servanzi, L. & Sibilla, S. (2022) Juvenile fish stranding induced by upstream gate operation: a risk assessment through eco-hydraulic modeling. *Ecological Engineering*, 183, 106753. Available from: <https://doi.org/10.1016/j.ecoleng.2022.106753>
- EU WFD, W. F. D. (2019) *Guidance document no. 37: steps for defining and assessing ecological potential for improving comparability of heavily modified water bodies common implementation strategy for the water framework directive (2000/60/EC)*. Helsinki: European Commission.
- Francalanci, S., Parker, G. & Solari, L. (2008) Effect of seepage-induced nonhydrostatic pressure distribution on bed-load transport and bed morphodynamics. *Journal of Hydraulic Engineering*, 134(4), 378–389. Available from: [https://doi.org/10.1061/\(ASCE\)0733-9429\(2008\)134:4\(378\)](https://doi.org/10.1061/(ASCE)0733-9429(2008)134:4(378))
- Gaeuman, D. (2014) High-flow gravel injection for constructing designed in-channel features. *River Research and Applications*, 30(6), 685–706. Available from: <https://doi.org/10.1002/rra.2662>
- Gillespie, B.R., Desmet, S., Kay, P., Tillotson, M.R. & Brown, L.E. (2015) A critical analysis of regulated river ecosystem responses to managed environmental flows from reservoirs. *Freshwater Biology*, 60(2), 410–425. Available from: <https://doi.org/10.1111/fwb.12506>
- Gostner, W. (2012) *The hydro-morphological index of diversity: a planning tool for river restoration projects*. In: EPFL-LCH.
- Gregory, A., Morrison, R.R. & Stone, M. (2018) Assessing the hydrogeomorphic effects of environmental flows using hydrodynamic modeling. *Environmental Management*, 62(2), 352–364. Available from: <https://doi.org/10.1007/s00267-018-1041-6>
- Grill, G., Lehner, B., Lumsdon, A.E., MacDonald, G.K., Zarfl, C. & Liermann, C.R. (2015) An index-based framework for assessing patterns and trends in river fragmentation and flow regulation by global dams at multiple scales. *Environmental Research Letters*, 10(1), 015001. Available from: <https://doi.org/10.1088/1748-9326/10/1/015001>
- Guan, M., Wright, N.G. & Sleigh, P.A. (2014) 2D process-based morphodynamic model for flooding by noncohesive dyke breach. *Journal of Hydraulic Engineering*, 140(7), 04014022. Available from: [https://doi.org/10.1061/\(ASCE\)HY.1943-7900.0000861](https://doi.org/10.1061/(ASCE)HY.1943-7900.0000861)
- Guan, M., Wright, N.G. & Sleigh, P.A. (2015) Multiple effects of sediment transport and geomorphic processes within flood events: modelling and understanding. *International Journal of Sediment Research*, 30(4), 371–381. Available from: <https://doi.org/10.1016/j.ijsrc.2014.12.001>
- Hassan, M.A., Egozi, R. & Parker, G. (2006) Experiments on the effect of hydrograph characteristics on vertical grain sorting in gravel bed rivers. *Water Resources Research*, 42(9), Available from: <https://doi.org/10.1029/2005WR004707>
- Hayes, D.S., Moreira, M., Boavida, I., Haslauer, M., Unfer, G., Zeiringer, B., et al. (2019) Life stage-specific hydropeaking flow rules. *Sustainability*, 11(6), 1547. Available from: <https://doi.org/10.3390/su11061547>
- Hsu, L., Finnegan, N.J. & Brodsky, E.E. (2011) A seismic signature of river bedload transport during storm events. *Geophysical Research Letters*, 38(13), n/a. Available from: <https://doi.org/10.1029/2011GL047759>
- James, M.R., Chandler, J.H., Eltner, A., Fraser, C., Miller, P.E., Mills, J.P., et al. (2019) Guidelines on the use of structure-from-motion photogrammetry in geomorphic research. *Earth Surface Processes and Landforms*, 44(10), 2081–2084. Available from: <https://doi.org/10.1002/esp.4637>
- Kaur, S., Horne, A.C., Nathan, R., Szemis, J.M., Gibson, L., Costa, A.M., et al. (2019) Examining trade-offs in piggybacking flow events while making environmental release decisions in a river system. *Journal of Water Resources Planning and Management*, 145(6), 04019019. Available from: [https://doi.org/10.1061/\(ASCE\)WR.1943-5452.0001048](https://doi.org/10.1061/(ASCE)WR.1943-5452.0001048)
- Kevic, M., Ortlepp, J., Mürle, U. & Robinson, C.T. (2018) Effects of experimental floods in two rivers with contrasting valley morphologies. *Fundamental and Applied Limnology/Archiv für Hydrobiologie*, 192(2), 145–160. Available from: <https://doi.org/10.1127/fal/2018/1177>
- Keylock, C.J., Constantinescu, G. & Hardy, R.J. (2012) The application of computational fluid dynamics to natural river channels: eddy resolving versus mean flow approaches. *Geomorphology*, 179, 1–20. Available from: <https://doi.org/10.1016/j.geomorph.2012.09.006>
- Konrad, C.P., Olden, J.D., Lytle, D.A., Melis, T.S., Schmidt, J.C., Bray, E.N., et al. (2011) Large-scale flow experiments for managing river systems. *Bioscience*, 61(12), 948–959. Available from: <https://doi.org/10.1525/bio.2011.61.12.5>
- Kozarek, J.L., Hession, W.C., Dolloff, C.A. & Diplas, P. (2010) Hydraulic complexity metrics for evaluating in-stream brook trout habitat. *Journal of Hydraulic Engineering*, 136(12), 1067–1076. Available from: [https://doi.org/10.1061/\(ASCE\)HY.1943-7900.0000197](https://doi.org/10.1061/(ASCE)HY.1943-7900.0000197)
- Lacey, R.J., Neary, V.S., Liao, J.C., Enders, E.C. & Tritico, H.M. (2012) The IPOS framework: linking fish swimming performance in altered flows from laboratory experiments to rivers. *River Research and Applications*, 28(4), 429–443. Available from: <https://doi.org/10.1002/rra.1584>
- Lane, S.N., Gentile, A. & Goldenschue, L. (2020) Combining UAV-based SfM-MVS photogrammetry with conventional monitoring to set environmental flows: modifying dam flushing flows to improve alpine stream habitat. *Remote Sensing*, 12(23), 3868. Available from: <https://doi.org/10.3390/rs12233868>
- Lane, B.A., Pasternack, G.B. & Sandoval Solis, S. (2018) Integrated analysis of flow, form, and function for river management and design testing. *Ecohydrology*, 11(5), e1969. Available from: <https://doi.org/10.1002/eco.1969>
- Lane, S.N., Westaway, R.M. & Murray Hicks, D. (2003) Estimation of erosion and deposition volumes in a large, gravel-bed, braided river using synoptic remote sensing. *Earth Surface Processes Landforms: the Journal of the British Geomorphological Research Group*, 28(3), 249–271. Available from: <https://doi.org/10.1002/esp.483>
- Lehner, B., Liermann, C.R., Revenga, C., Vörösmarty, C., Fekete, B., Couzet, P., et al. (2011) High-resolution mapping of the world's reservoirs and dams for sustainable river-flow management. *Frontiers in Ecology and the Environment*, 9(9), 494–502. Available from: <https://doi.org/10.1890/100125>
- Lenzi, M.A. & Marchi, L. (2000) Suspended sediment load during floods in a small stream of the dolomites (northeastern Italy). *Catena*, 39(4), 267–282. Available from: [https://doi.org/10.1016/S0341-8162\(00\)00079-5](https://doi.org/10.1016/S0341-8162(00)00079-5)
- Lessard, J., Hicks, D.M., Snelder, T.H., Arscott, D.B., Larned, S.T., Booker, D., et al. (2013) Dam design can impede adaptive management of environmental flows: a case study from the Opuha Dam,

- New Zealand. *Environmental Management*, 51(2), 459–473. Available from: <https://doi.org/10.1007/s00267-012-9971-x>
- Lesser, G.R., Roelvink, J.A. van Kester, J.T. & Stelling, G.S. (2004) Development and validation of a three-dimensional morphological model. *Coastal Engineering*, 51(8–9), 883–915. Available from: <https://doi.org/10.1016/j.coastaleng.2004.07.014>
- Li, S. & Duffy, C.J. (2011) Fully coupled approach to modeling shallow water flow, sediment transport, and bed evolution in rivers. *Water Resources Research*, 47(3), Available from: <https://doi.org/10.1029/2010WR009751>
- Li, M., Shi, X., Jin, Z., Ke, S., Lin, C., An, R., et al. (2020) Behaviour and ability of a cyprinid (*Schizopygopsis youngusbandi*) to cope with accelerating flows when migrating downstream. *River Research and Applications*, 37(8), 1168–1179. Available from: <https://doi.org/10.1002/rra.3686>
- Li, W., van Maren, D.S., Wang, Z.B., de Vriend, H.J. & Wu, B. (2014) Peak discharge increase in hyperconcentrated floods. *Advances in Water Resources*, 67, 65–77. Available from: <https://doi.org/10.1016/j.advwatres.2014.02.007>
- Li, H., Yang, G., Ma, J., Wei, Y., Kang, L., He, Y., et al. (2019) The role of turbulence in internal phosphorus release: turbulence intensity matters. *Environmental Pollution*, 252(Pt A), 84–93. Available from: <https://doi.org/10.1016/j.envpol.2019.05.068>
- Liedermann, M., Gmeiner, P., Kreisler, A., Tritthart, M. & Habersack, H. (2018) Insights into bedload transport processes of a large regulated gravel-bed river. *Earth Surface Processes and Landforms*, 43(2), 514–523. Available from: <https://doi.org/10.1002/esp.4253>
- Loire, R., Grosprêtre, L., Malavoi, J.-R., Ortiz, O. & Piégay, H. (2019) What discharge is required to remove silt and sand downstream from a dam? An adaptive approach on the Selves River France. *Watermark*, 11(2), 392. Available from: <https://doi.org/10.3390/w11020392>
- Loire, R., Piégay, H., Malavoi, J.R., Beche, L., Dumoutier, Q., Mosseri, J., et al. (2019) Unclogging improvement based on interdate and interreach comparison of water release monitoring (Durance, France). *River Research and Applications*, 35(8), 1107–1118. Available from: <https://doi.org/10.1002/rra.3489>
- Magdaleno, F. (2017) Experimental floods: a new era for Spanish and Mediterranean rivers? *Environmental Science & Policy*, 75, 10–18. Available from: <https://doi.org/10.1016/j.envsci.2017.05.011>
- Manual, S. (2019) *Surface velocity radar user's manual*. Available from: <https://www.decatureurope.com/>. [Accessed 10th September 2019].
- Mao, L. (2012) The effect of hydrographs on bed load transport and bed sediment spatial arrangement. *Journal of Geophysical Research - Earth Surface*, 117(F3), Available from: <https://doi.org/10.1029/2012JF002428>
- Meyer-Peter, E., and Müller, R. (1948). *Formulas for bed-load transport*. Proceedings of 2nd meeting of the International Association for Hydraulic Structures Research. Stockholm: IAHR, appendix 2.
- Moreira, M., Hayes, D.S., Boavida, I., Schletterer, M., Schmutz, S. & Pinheiro, A. (2019) Ecologically-based criteria for hydropeaking mitigation: a review. *Science of the Total Environment*, 657, 1508–1522. Available from: <https://doi.org/10.1016/j.scitotenv.2018.12.107>
- Moretto, J., Rigon, E., Mao, L., Delai, F., Picco, L. & Lenzi, M.A. (2014) Short-term geomorphic analysis in a disturbed fluvial environment by fusion of LiDAR, colour bathymetry and dGPS surveys. *Catena*, 122, 180–195. Available from: <https://doi.org/10.1016/j.catena.2014.06.023>
- Mürle, U., Ortlepp, J. & Zahner, M. (2003) Effects of experimental flooding on riverine morphology, structure and riparian vegetation: the river Spöl, Swiss National Park. *Aquatic Sciences*, 65(3), 191–198. Available from: <https://doi.org/10.1007/s00027-003-0665-6>
- Newson, M.D. & Newson, C.L. (2000) Geomorphology, ecology and river channel habitat: mesoscale approaches to basin-scale challenges. *Progress in Physical Geography*, 24(2), 195–217. Available from: <https://doi.org/10.1177/030913330002400203>
- Nilsson, C., Reidy, C.A., Dynesius, M. & Revenga, C. (2005) Fragmentation and flow regulation of the world's large river systems. *Science*, 308(5720), 405–408. Available from: <https://doi.org/10.1126/science.1107887>
- Ortlepp, J. & Mürle, U. (2003) Effects of experimental flooding on brown trout (*Salmo trutta fario* L.): the river Spöl, Swiss National Park. *Aquatic Sciences*, 65(3), 232–238. Available from: <https://doi.org/10.1007/s00027-003-0666-5>
- Parasiewicz, P. (2007) The MesoHABSIM model revisited. *River Research and Applications*, 23(8), 893–903. Available from: <https://doi.org/10.1002/rra.1045>
- Parker, G. (1990) Surface-based bedload transport relation for gravel rivers. *Journal of Hydraulic Research*, 28(4), 417–436. Available from: <https://doi.org/10.1080/00221689009499058>
- Pasternack, G.B., Wang, C.L. & Merz, J.E. (2004) Application of a 2D hydrodynamic model to design of reach-scale spawning gravel replenishment on the Mokelumne River, California. *River Research and Applications*, 20(2), 205–225. Available from: <https://doi.org/10.1002/rra.748>
- Patten, D.T., Harpman, D.A., Voita, M.I. & Randle, T.J. (2001) A managed flood on the Colorado River: background, objectives, design, and implementation. *Ecological Applications*, 11(3), 635–643. Available from: [https://doi.org/10.1890/1051-0761\(2001\)011\[0635:AMFOTC\]2.0.CO;2](https://doi.org/10.1890/1051-0761(2001)011[0635:AMFOTC]2.0.CO;2)
- Pfeifer, N. (2008) *DSM/DTM filtering*. International school on lidar technology 2008. India: IIT Kanpur Available at: <http://www.iitk.ac.in/>
- Pfeiffer, A.M., Collins, B.D., Anderson, S.W., Montgomery, D.R. & Istanbuloglu, E. (2019) River bed elevation variability reflects sediment supply, rather than peak flows, in the uplands of Washington State. *Water Resources Research*, 55(8), 6795–6810. Available from: <https://doi.org/10.1029/2019WR025394>
- Phillips, C., Hill, K.M., Paola, C., Singer, M. & Jerolmack, D. (2018) Effect of flood hydrograph duration, magnitude, and shape on bed load transport dynamics. *Geophysical Research Letters*, 45(16), 8264–8271. Available from: <https://doi.org/10.1029/2018GL078976>
- Pitt, J. & Kendy, E. (2017) Shaping the 2014 Colorado River Delta pulse flow: rapid environmental flow design for ecological outcomes and scientific learning. *Ecological Engineering*, 106, 704–714. Available from: <https://doi.org/10.1016/j.ecoleng.2016.12.002>
- Poff, N.L. (2018) Beyond the natural flow regime? Broadening the hydro-ecological foundation to meet environmental flows challenges in a non-stationary world. *Freshwater Biology*, 63(8), 1011–1021. Available from: <https://doi.org/10.1111/fwb.13038>
- Poff, N.L., Allan, J.D., Bain, M.B., Karr, J.R., Prestegard, K.L., Richter, B.D., et al. (1997) The natural flow regime. *Bioscience*, 47(11), 769–784. Available from: <https://doi.org/10.2307/1313099>
- Prancevic, J.P. & Lamb, M.P. (2015) Unraveling bed slope from relative roughness in initial sediment motion. *Journal of Geophysical Research - Earth Surface*, 120(3), 474–489. Available from: <https://doi.org/10.1002/2014JF003323>
- Rainato, R., Mao, L. & Picco, L. (2018) Near-bankfull floods in an Alpine stream: effects on the sediment mobility and bedload magnitude. *International Journal of Sediment Research*, 33(1), 27–34. Available from: <https://doi.org/10.1016/j.ijrsr.2017.03.006>
- Richter, B.D. (2010) Re-thinking environmental flows: from allocations and reserves to sustainability boundaries. *River Research and Applications*, 26(8), 1052–1063. Available from: <https://doi.org/10.1002/rra.1320>
- Robinson, C.T. (2012) Long-term changes in community assembly, resistance, and resilience following experimental floods. *Ecological Applications*, 22(7), 1949–1961. Available from: <https://doi.org/10.1890/11-1042.1>
- Robinson, C.T., Siebers, A.R. & Ortlepp, J. (2018) Long-term ecological responses of the River Spöl to experimental floods. *Freshwater Science*, 37(3), 433–447. Available from: <https://doi.org/10.1086/699481>
- Rose, T., Erskine, W. & Miners, B. (2020) Channel recovery in a regulated river: effects of an experimental and natural flood in the Snowy River, SE Australia. *River Research and Applications*, 36(4), 567–579. Available from: <https://doi.org/10.1002/rra.3452>
- Rueda, L.V.A. (2015) *Turbulence, sediment transport, erosion, and sandbar beach failure processes in grand*. Canyon: Arizona State University.
- Ruiz-Villanueva, V., Aarnink, J., Gibaja del Hoyo, J., Finch, B. & Vuaridel, M. (2022) *Integrating flow-, sediment- and instream wood-regimes during*

- e-flows in the Spöl River (Swiss Alps)*. Paper presented at the Conference: 39th IAHR World Congress. Granada, Spain: IAHR.
- Sammartano, G., and Spanò, A. (2016). *DEM generation based on UAV photogrammetry data in critical areas*. Paper presented in the 2nd International Conference on Geographical Information Systems Theory, Applications and Management (GISTAM), pp. 92–98.
- Scheurer, T. & Molinari, P. (2003) Experimental floods in the River Spöl, Swiss National Park: framework, objectives and design. *Aquatic Sciences*, 65(3), 183–190. Available from: <https://doi.org/10.1007/s00027-003-0667-4>
- Schlosser, I.J. (1995) Critical landscape attributes that influence fish population dynamics in headwater streams. *Hydrobiologia*, 303(1), 71–81. Available from: <https://doi.org/10.1007/BF00034045>
- Schlunegger, F. & Garefalakis, P.E. (2018) Clast imbrication in coarse-grained mountain streams and stratigraphic archives as indicator of deposition in upper flow regime conditions. *Earth Surface Dynamics*, 6(3), 743–761. Available from: <https://doi.org/10.5194/esurf-6-743-2018>
- Schmidt, J.C., Parnell, R.A., Grams, P.E., Hazel, J.E., Kaplinski, M.A., Stevens, L.E., et al. (2001) The 1996 controlled flood in Grand Canyon: flow, sediment transport, and geomorphic change. *Ecological Applications*, 11(3), 657–671. Available from: [https://doi.org/10.1890/1051-0761\(2001\)011\[0657:TCFIGC\]2.0.CO;2](https://doi.org/10.1890/1051-0761(2001)011[0657:TCFIGC]2.0.CO;2)
- Shafroth, P.B., Wilcox, A.C., Lytle, D.A., Hickey, J.T., Andersen, D.C., Beauchamp, V.B., et al. (2010) Ecosystem effects of environmental flows: modelling and experimental floods in a dryland river. *Freshwater Biology*, 55(1), 68–85. Available from: <https://doi.org/10.1111/j.1365-2427.2009.02271.x>
- Shields, A. (1936) *Application of similarity principles and turbulence research to bed-load movement*. California: Soil Conservation Service Cooperative Laboratory California Institute of Technology Pasadena.
- Silva, A.T., Bærum, K.M., Hedger, R.D., Baktoft, H., Fjeldstad, H.-P., Gjelland, K.Ø., et al. (2020) The effects of hydrodynamics on the three-dimensional downstream migratory movement of Atlantic salmon. *Science of the Total Environment*, 705, 135773. Available from: <https://doi.org/10.1016/j.scitotenv.2019.135773>
- Simpson, G. & Castellort, S. (2006) Coupled model of surface water flow, sediment transport and morphological evolution. *Computers & Geosciences*, 32(10), 1600–1614. Available from: <https://doi.org/10.1016/j.cageo.2006.02.020>
- Smith, M.W., Carrivick, J.L., Hooke, J. & Kirkby, M.J. (2014) Reconstructing flash flood magnitudes using 'structure-from-motion': a rapid assessment tool. *Journal of Hydrology*, 519, 1914–1927. Available from: <https://doi.org/10.1016/j.jhydrol.2014.09.078>
- Stähly, S., Franca, M.J., Robinson, C.T. & Schleiss, A.J. (2020) Erosion, transport and deposition of a sediment replenishment under flood conditions. *Earth Surface Processes and Landforms*, 45(13), 3354–3367. Available from: <https://doi.org/10.1002/esp.4970>
- Staines, K.E. & Carrivick, J.L. (2015) Geomorphological impact and morphodynamic effects on flow conveyance of the 1999 jökulhlaup at sólheimajökull, Iceland. *Earth Surface Processes Landforms: the Journal of the British Geomorphological Research Group*, 40(10), 1401–1416. Available from: <https://doi.org/10.1002/esp.3750>
- Stewardson, M.J., Acreman, M., Costelloe, J.F., Fletcher, T.D., Fowler, K.J., Horne, A.C., et al. (2017) Understanding hydrological alteration. In: *Water for the environment*. Academic Press (imprint of Elsevier), pp. 37–64 <https://doi.org/10.1016/B978-0-12-803907-6.00003-6>
- Tamminga, A.D., Eaton, B.C. & Hugenholtz, C.H. (2015) UAS-based remote sensing of fluvial change following an extreme flood event. *Earth Surface Processes and Landforms*, 40(11), 1464–1476. Available from: <https://doi.org/10.1002/esp.3728>
- Tavelli, M., Piccolroaz, S., Stradiotti, G., Pisaturo, G.R. & Righetti, M. (2020) A new mass-conservative, two-dimensional, semi-implicit numerical scheme for the solution of the Navier-Stokes equations in gravel bed rivers with erodible fine sediments. *Watermark*, 12(3), 690. Available from: <https://doi.org/10.3390/w12030690>
- Uehlinger, U., Kawecka, B. & Robinson, C.T. (2003) Effects of experimental floods on periphyton and stream metabolism below a high dam in the Swiss Alps (River Spöl). *Aquatic Sciences*, 65(3), 199–209. Available from: <https://doi.org/10.1007/s00027-003-0664-7>
- Van Appledorn, M., Baker, M.E. & Miller, A.J. (2019) River-valley morphology, basin size, and flow-event magnitude interact to produce wide variation in flooding dynamics. *Ecosphere*, 10(1), e02546. Available from: <https://doi.org/10.1002/ecs2.2546>
- Van Rijn, L.C. (1984) Sediment transport, part I: bed load transport. *Journal of hydraulic engineering*, 110(10), 1431–1456.
- Vanzo, D., Zolezzi, G. & Siviglia, A. (2016) Eco-hydraulic modelling of the interactions between hydropeaking and river morphology. *Ecohydrology*, 9(3), 421–437. Available from: <https://doi.org/10.1002/eco.1647>
- Welber, M., Le Coz, J., Laronne, J.B., Zolezzi, G., Zamler, D., Dramais, G., et al. (2016) Field assessment of noncontact stream gauging using portable surface velocity radars (SVR). *Water Resources Research*, 52(2), 1108–1126. Available from: <https://doi.org/10.1002/2015WR017906>
- Welcomme, R.L. & Halls, A. (2004) *Dependence of tropical river fisheries on flow*. In Proceedings of the second international symposium on the management of large rivers for fisheries, 2 vols. RAP Publication 2004/16. Food and Agriculture Organization of the United Nations (FAO), pp. 267–283.
- Westoby, M., Brasington, J., Glasser, N., Hambrey, M. & Reynolds, J. (2012) Structure-from-motion photogrammetry: a novel, low-cost tool for geomorphological applications. *Geomorphology*, 179, 300–314. Available from: <https://doi.org/10.1016/j.geomorph.2012.08.021>
- Whipple, A.A. & Viers, J.H. (2019) Coupling landscapes and river flows to restore highly modified rivers. *Water Resources Research*, 55(6), 4512–4532. Available from: <https://doi.org/10.1029/2018WR022783>
- Wilcock, P.R. & Crowe, J.C. (2003) Surface-based transport model for mixed-size sediment. *Journal of Hydraulic Engineering*, 129(2), 120–128. Available from: [https://doi.org/10.1061/\(ASCE\)0733-9429\(2003\)129:2\(120\)](https://doi.org/10.1061/(ASCE)0733-9429(2003)129:2(120))
- Wilkes, M.A., Maddock, I., Visser, F. & Acreman, M.C. (2013) Incorporating hydrodynamics into ecohydraulics: the role of turbulence in the swimming performance and habitat selection of stream-dwelling fish. *Ecohydraulics: an Integrated Approach*. Oxford: Wiley Blackwell.
- Wohl, E., Bledsoe, B.P., Jacobson, R.B., Poff, N.L., Rathburn, S.L., Walters, D.M., et al. (2015) The natural sediment regime in rivers: broadening the foundation for ecosystem management. *Bioscience*, 65(4), 358–371. Available from: <https://doi.org/10.1093/biosci/biv002>
- Wohl, E.E. & Cenderelli, D.A. (2000) Sediment deposition and transport patterns following a reservoir sediment release. *Water Resources Research*, 36(1), 319–333. Available from: <https://doi.org/10.1029/1999WR900272>
- Wong, J.S., Freer, J.E., Bates, P.D., Sear, D.A. & Stephens, E.M. (2015) Sensitivity of a hydraulic model to channel erosion uncertainty during extreme flooding. *Hydrological Processes*, 29(2), 261–279. Available from: <https://doi.org/10.1002/hyp.10148>
- Wood, P.J. (2005) The response of four lotic macroinvertebrate taxa to burial by sediments. *Archiv für Hydrobiologie*, 163(2), 145–162. Available from: <https://doi.org/10.1127/0003-9136/2005/0163-0145>
- Woodget, A.S., Austrums, R., Maddock, I.P. & Habit, E. (2017) Drones and digital photogrammetry: from classifications to continuums for monitoring river habitat and hydromorphology. *Wiley interdisciplinary reviews. Watermark*, 4(4), e1222. Available from: <https://doi.org/10.1002/wat2.1222>
- Wright, S.A. & Kaplinski, M. (2011) Flow structures and sandbar dynamics in a canyon river during a controlled flood, Colorado River, Arizona. *Journal of Geophysical Research - Earth Surface*, 116(F1), n/a. Available from: <https://doi.org/10.1029/2009JF001442>
- Wyrick, J.R., Senter, A.E. & Pasternack, G.B. (2014) Revealing the natural complexity of fluvial morphology through 2D hydrodynamic delineation of river landforms. *Geomorphology*, 210, 14–22. Available from: <https://doi.org/10.1016/j.geomorph.2013.12.013>

- Xia, J., Lin, B., Falconer, R.A. & Wang, G. (2010) Modelling dam-break flows over mobile beds using a 2D coupled approach. *Advances in Water Resources*, 33(2), 171–183. Available from: <https://doi.org/10.1016/j.advwatres.2009.11.004>
- Yarnell, S.M., Petts, G.E., Schmidt, J.C., Whipple, A.A., Beller, E.E., Dahm, C.N., et al. (2015) Functional flows in modified riverscapes: hydrographs, habitats and opportunities. *Bioscience*, 65(10), 963–972. Available from: <https://doi.org/10.1093/biosci/biv102>
- Zietara, A.M. (2017) *Creating digital elevation model (DEM) based on ground points extracted from classified aerial images obtained from unmanned aerial vehicle (UAV)*. Master's thesis. Trondheim, Norway: Norwegian University of Science and Technology. Available at: <https://ntnuopen.ntnu.no/ntnu-xmlui/handle/11250/2452455> Accessed: 20 May 2021.

SUPPORTING INFORMATION

Additional supporting information can be found online in the Supporting Information section at the end of this article.

How to cite this article: Hashemi, S., Carrivick, J. & Klaar, M. (2024) Hydromorphological response of heavily modified rivers to flood releases from reservoirs: A case study of the Spöl River, Switzerland. *Earth Surface Processes and Landforms*, 49(3), 1028–1046. Available from: <https://doi.org/10.1002/esp.5749>